

Adiabatic Eastern Boundary Currents

PAOLA CESSI AND CHRISTOPHER L. WOLFE

Scripps Institution of Oceanography, University of California, San Diego, La Jolla, California

(Manuscript received 22 October 2012, in final form 3 February 2013)

ABSTRACT

The dynamics of the eastern boundary current of a high-resolution, idealized model of oceanic circulation are analyzed and interpreted in terms of residual mean theory. In this framework, it is clear that the eastern boundary current is adiabatic and inviscid. Nevertheless, the time-averaged potential vorticity is not conserved along averaged streamlines because of the divergence of Eliassen–Palm fluxes, associated with buoyancy and momentum eddy fluxes. In particular, eddy fluxes of buoyancy completely cancel the mean downwelling or upwelling, so that there is no net diapycnal residual transport. The eddy momentum flux acts like a drag on the mean velocity, opposing the acceleration from the eddy buoyancy flux: in the potential vorticity budget this results in a balance between the divergences of eddy relative vorticity and buoyancy fluxes, which leads to a baroclinic eastern boundary current whose horizontal scale is the Rossby deformation radius and whose vertical extent depends on the eddy buoyancy transport, the Coriolis parameter, and the mean surface buoyancy distribution.

1. Introduction

Near the eastern boundaries of the oceans, the wind stress is partially constrained by encounter with continents (Rienecker and Ehret 1988), where the wind acquires a meridional component that generates zonal Ekman transport, accompanied by upwelling (or downwelling). In addition, the deceleration of wind stress as the coast is approached, together with the aforementioned wind steering, produces a pattern of increased Ekman suction (or pumping), which can also lead to upwelling (or downwelling). Because of the important implications to fisheries, much of the focus on coastal circulation has been on near-surface upwelling and the associated equatorward currents, which we believe arise because of the local wind stress effect. However, all of the eastern boundary current (EBC) systems also have poleward undercurrents—usually faster than the surface equatorward flow—overlying a deeper equatorward current (Barton 1998; Pierce et al. 2000; Penven et al. 2005). In some regions the poleward EBC is found at the surface, overwhelming the surface equatorward current

induced by the upwelling-favorable winds, as is the case for the Leeuwin Current (Smith et al. 1991).

In this study we show that the poleward current, accompanied by a deeper equatorward current, is the eastern boundary expression of the large-scale wind-driven circulation in the subtropical and subpolar regions. Without a near-shore meridional component of the wind stress there is no surface equatorward current near the eastern boundary that rides over the poleward component of the EBC.

Other studies have reached the same conclusion. In particular, with a series of idealized numerical experiments, Godfrey and Weaver (1991) have shown that an important element for a substantial poleward EBC (overlying a deeper equatorward undercurrent) is the existence of a large-scale latitudinal buoyancy gradient, which, if strong enough, can overwhelm the local wind stress effects all the way to the surface. However, these numerical experiments are at a coarse resolution, which does not allow the development of mesoscale eddies. Observations (Todd et al. 2011) and high-resolution model experiments (Marchesiello et al. 2003) have demonstrated that EBCs are embedded in a vigorous eddy field and clearly emerge only after an appropriate time average. Regional eddy-resolving simulations include forcing and geometry (e.g., coastline and bottom relief) that are as realistic as possible and do not permit teasing

Corresponding author address: Paola Cessi, Scripps Institution of Oceanography, University of California, San Diego, 9500 Gilman Dr., Mail Code 0213, La Jolla, CA 92093-0213.
E-mail: pcessi@ucsd.edu

apart what aspects of the currents are extrinsically induced and which are from intrinsic dynamics. For example, is the cross-shore scale of the EBC set by the scale of the alongshore wind, by the width of the shelf, or by internal dynamics? Is it necessary to have alongshore winds to have an EBC? In the following, it is shown that EBCs are part of the general circulation of the ocean: they are found without local alongshore winds or topographic features.

Classical theories of the ocean's general circulation assume that the eastern boundary is the region of weakest subsurface flow. Specifically, laminar thermocline theories confine the motion near the eastern boundary of the surface, with the subsurface near-shore region at rest: this is the "shadow-zone" of Luyten et al. (1983) or the "blocked region" of Rhines and Young (1982). This region is required by the condition of no alongshore pressure gradient at the solid boundary, so that there is no geostrophic flow into the wall. This configuration implies that the meridional buoyancy gradients are squeezed into a region whose thickness vanishes on the eastern boundary, creating a singularity in the buoyancy field. It is thus not surprising that an energetic field of eddies spontaneously develops in response to the singular density gradient predicted by laminar theories. In turn, the eddy fluxes of buoyancy and momentum break the geostrophic constraint in an inviscid and adiabatic fashion, driving an across-shore pressure gradient that supports the EBC. Here, we illustrate the resulting EBC and its connection to the general circulation of the ocean in a simple geometry and for idealized large-scale wind and buoyancy forcing.

Contrary to the assumption of classical theories, EBC have alongshore pressure and buoyancy gradients (Godfrey and Ridgway 1985; Chapman and Lentz 2005); although the alongshore velocity in EBC systems is in geostrophic balance, and thus not directly related to the meridional pressure gradient, various frictional processes (lateral friction, vertical friction, or bottom drag) have been advocated to justify the balance between the alongshore pressure gradient and the EBC. In the following, we will show that there is no need to invoke viscous processes in the EBC and that a boundary current can be obtained with inviscid dynamics. However, eddy processes are essential and in particular the across-shore eddy transport of buoyancy and momentum balances the alongshore pressure gradient, in accordance with observations of the Leeuwin Current (Feng et al. 2005). Eddy fluxes of buoyancy and momentum are often parameterized as downgradient diffusion and viscosity, respectively, and in this sense there is a connection between the laminar, frictional theories, and the eddy-resolving results. We find that the mean boundary

currents obtained in the eddy-resolving context are of larger amplitude than those obtained in laminar, viscous theories, and that their scale is much larger than the thickness of the lateral Ekman layer.

Laminar theories that account for the alongshore pressure gradient have to relax some of the idealized assumptions, for example by assuming that frictional and/or diabatic effects become important as the eastern boundary is approached. In particular, several authors have assumed that diabatic mixing is a dominant process throughout the region of alongshore gradients (McCreary 1981; Colin de Verdière 1989; Sumata and Kubokawa 2001). Sumata and Kubokawa (2001) showed that the region containing the horizontal gradient near the eastern boundary is a deep mixed layer where density is vertically homogenized by the strong downwelling of the impinging eastward flow near the eastern boundary, balanced by mixing. Schloesser et al. (2012) interpret the eastern boundary solution of Sumata and Kubokawa (2001) as an adiabatic process where the flow is oriented along the quasi-vertical isopycnals. It is not clear whether in the solution of Sumata and Kubokawa (2001) diapycnal mixing is important or negligible because neither Sumata and Kubokawa (2001) nor Schloesser et al. (2012) present buoyancy diagnostics to clarify whether the mean vertical advection is primarily balanced by mean horizontal advection (e.g., adiabatic dynamics) or by mixing processes (e.g., diabatic dynamics). Because of the neglect of eddy processes, these are the only balances possible in laminar models.

In our study we find that the region of alongshore buoyancy and pressure gradients next to the eastern boundary is quasi-adiabatic, and that the advection from the mean downwelling is compensated by the eddy flux of buoyancy. This balance leads to a sloping buoyancy profile: the eddy buoyancy flux restratifies the fluid against the action of the mean vertical velocity. This eddy flux of buoyancy also provides an acceleration of the time-mean meridional flow, which is halted by the eddy momentum flux, resulting in a net baroclinic meridional EBC.

The constraint that the circulation remains adiabatic and inviscid all the way to the eastern boundary, while relaxing the assumption of laminar flow, provides a scaling for the width of the EBC and the depth through which the alongshore pressure gradients act. Because of the importance of eddy fluxes, these scales depend on the statistics of the eddy field, which are not easily related to the properties of the statistically steady flow. As detailed below, this study differs from our previous attempts to construct a theory of EBC, which includes the rectified effect of eddies (Cessi and Wolfe 2009a; Cessi et al. 2010) in that the dynamics are adiabatic and eddy momentum flux is important.

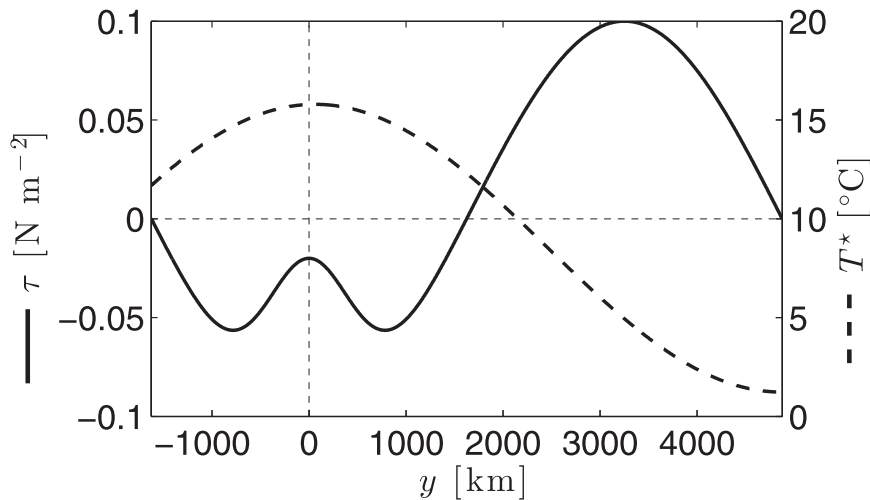


FIG. 1. The zonal component of the wind stress τ (solid line) and the relaxation temperature T^* (dashed line) as a function of y .

The approach taken here is to consider a simple geometrical configuration, both in terms of the domain and the shape of the forcing, while allowing a grid size sufficient to resolve mesoscale (but not submesoscale) features, in a domain large enough to allow basin-scale gyral circulation.

2. Configuration for high-resolution computations

The model used is the Massachusetts Institute of Technology General Circulation Model (MITgcm) configured as a closed box that comprises one and one-quarter hemispheres. The overall dimensions of the domain are 2400 km \times 6500 km \times 2000 m, with four-fifths of the domain in the Northern Hemisphere. The horizontal resolution is 5.4 km in the interior, increased over the 125 km nearest to the boundaries, with maximum resolution of 1 km at the boundary. There are 20 unequally spaced levels in the vertical, with vertical spacing increasing with depth ranging from 12 m at the surface to 225 m at the bottom.

There is no salt and the buoyancy b is determined by temperature θ through the linear equation of state $b = g\alpha\theta$, with $g\alpha = 2 \times 10^{-3} \text{ m s}^{-2} \text{ K}^{-1}$. Forcing is applied at the surface in the form of wind stress $\tau(y)$ in the zonal direction x and rapid relaxation to a prescribed temperature profile $T^*(y)$ (relaxation time is 11 days). Both τ and the relaxation to T^* are applied in the top level of the domain, and they are functions of latitude y only. There is no wind stress in the north–south direction. The profiles of surface buoyancy and east–west wind stress are shown in Fig. 1. The boundary conditions on the solid walls are “no normal flow” and “no slip.” The lateral viscosity is $\nu = 12 \text{ m}^2 \text{ s}^{-1}$ and the fourth-order

hyperviscosity $\nu_4 = 9 \times 10^7 \text{ m}^4 \text{ s}^{-1}$. The vertical viscosity is $\nu_v = 3 \times 10^{-4} \text{ m}^2 \text{ s}^{-1}$. Unlike typical general circulation models, the temperature diffusivity is isotropic with a value of $\kappa_v = 4 \times 10^{-5} \text{ m}^2 \text{ s}^{-1}$: this choice ensures that the diffusive flux is antiparallel to the buoyancy gradient. The model uses the flux-limiting advection scheme [a multidimensional implementation of the one-step, seventh-order, monotonicity-preserving scheme of Daru and Tenaud (2003)], with numerical diffusion smaller than that explicitly prescribed. The model is in Cartesian coordinates, on a β plane, with $\beta = 2 \times 10^{-11} \text{ m}^{-1} \text{ s}^{-1}$.

The model is integrated for 150 years, starting from an initial condition at lower resolution, which had reached a statistical steady state. This procedure ensures that a statistical steady state is reached, which is independent of the initial condition. Time averages are computed over the final 11 years of the integration.

Figure 2 shows the sea surface height (SSH) and the sea surface temperature (SST). The SSH pattern is indicative of the surface geostrophic velocity, which results from the superposition of the wind-driven circulation and the buoyancy-driven flow. The former gives a clear subtropical gyre, a subpolar gyre squeezed against the northwestern corner of the domain, and another cyclonic gyre in the tropics. The SSH isolines north of $y = 2000 \text{ km}$ show a steep northward turn near the eastern boundary where the surface expression of the subtropical/subpolar EBC is found.

The SST generally decreases poleward except for a region of weak gradient reversal near the equator. Close inspection of the SST reveals a steep poleward turn in a narrow region the eastern boundary of the subtropical and subpolar gyres: this is the location of a surface

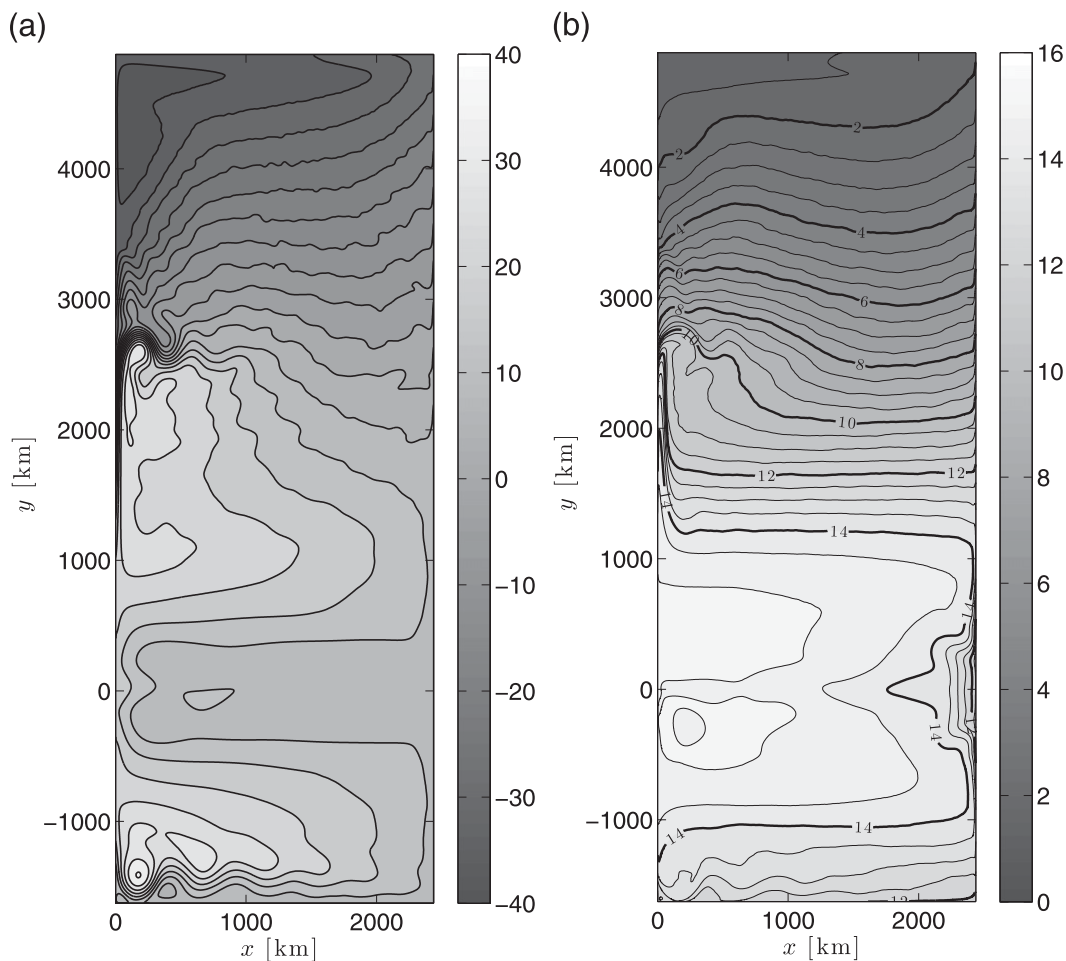


FIG. 2. (a) SSH (cm) and (b) SST ($^{\circ}$ C) as a function of x and y (km).

poleward EBC. Conversely, SSTs steeply turn equatorward in the tropical region, where the surface EBC is equatorward.

3. Phenomenology of the eastern boundary currents

We visualize the structure of the eastern boundary current in several ways. First, the Eulerian transport within 50 km of the boundary is contoured in the y - z plane (Fig. 3): the meridional transport (Fig. 3a) shows a surface poleward current north of $y = 1800$ km flowing above an equatorward current whose depth increases poleward; the Eulerian-mean vertical transport (Fig. 3b) is dominated by downwelling, which also deepens poleward. South of about $y = 1800$ km, the sign of the meridional currents is inverted, and equatorward of about $y = 1200$ km upwelling, rather than downwelling, is found at the surface.

Also shown is the temperature on the eastern boundary (Fig. 3b, thin lines): the horizontal gradients

are contained in the region of downwelling, and outside of this region the temperature is nearly independent of latitude. The boundary between these two regions, denoted by the thick line in Fig. 3a is the maximum in buoyancy frequency, $N^2 \equiv b_z$ (cf. Fig. 4), indicating that buoyancy would be discontinuous in the nondiffusive limit. This property has been exploited by Sumata and Kubokawa (2001) to derive an expression for the position of the internal boundary $h(y)$, separating the regions with and without latitudinal buoyancy gradients on the eastern boundary. In other words, it is assumed that the vertically averaged flow is geostrophically balanced, so that at the eastern boundary

$$\int_{-h(y)}^0 p_y dz = 0. \quad (1)$$

Assuming that the pressure is in hydrostatic balance and that, for $z > -h(y)$, the buoyancy is vertically homogeneous, Sumata and Kubokawa (2001) find

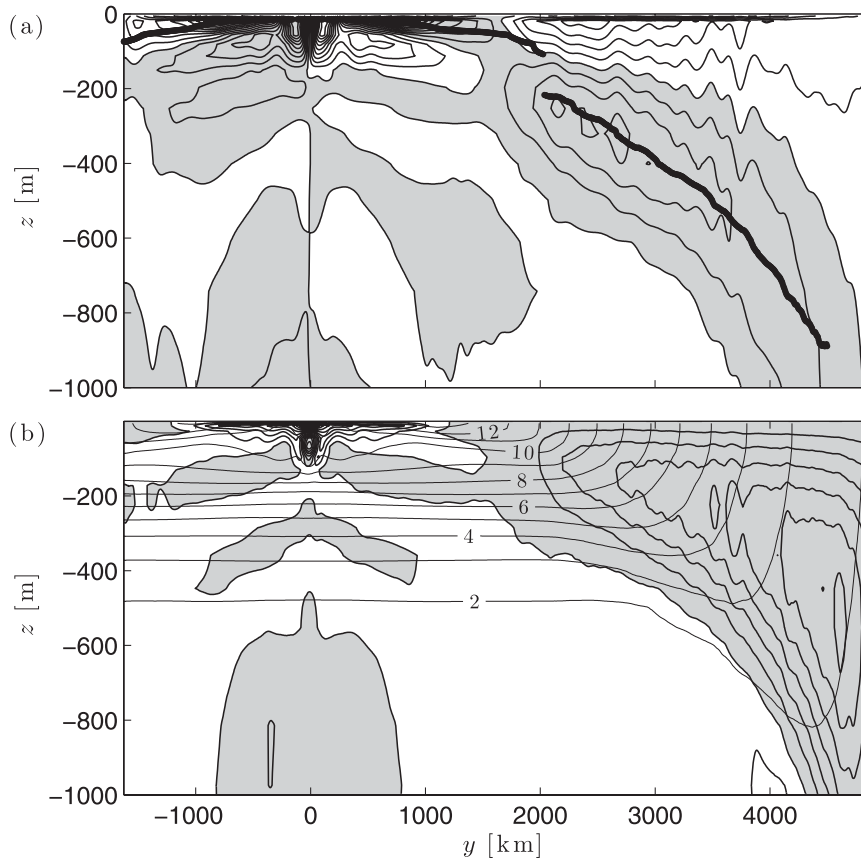


FIG. 3. (a) Meridional [contour interval (CI): $1000 \text{ m}^2 \text{ s}^{-1}$] and (b) vertical (CI: $0.5 \text{ m}^2 \text{ s}^{-1}$) time-averaged transport per unit depth integrated over the 50 km nearest to the eastern boundary and contoured as a function of y and z . Both fields have been smoothed with a Helmholtz filter, given by the solution F of the equation $F - l^2 F_{yy} = \text{field}$, with Neumann boundary conditions, and $l = 50 \text{ km}$. The time-averaged temperature on the eastern boundary is contoured in (b) (thin lines) and the position of the maximum of $N^2 \equiv \bar{b}_z$ is shown in (a) (thick line).

$$p = (z + h)b_s(y) - hb_A(-h), \quad (2)$$

which ensures a continuity of pressure at $z = -h$, despite the jump in density. Here, b_s denotes the surface buoyancy, and $b_A(z)$ indicates the abyssal resting stratification found for $z < -h$. Substituting (2) in (1) give the following relation for h :

$$h_y = \frac{h}{2} \frac{b_{sy}(y)}{b_A(-h) - b_s(y)}. \quad (3)$$

In our particular configuration, with no high-latitude region in the Southern Hemisphere, there is no abyssal stratification, and b_A is a constant equal to the minimum of b_s . In this case, it is possible to integrate (3) to obtain

$$h = h_o \sqrt{\frac{b_s(y_o) - b_A}{b_s(y) - b_A}}, \quad (4)$$

where h_o is the value of h at the latitude y_o . In other words, h must be specified somewhere (here at $y = y_o$) on the eastern boundary because the expression (3) contains no vertical scale related to the external parameters. Thus, the maintenance of horizontal gradients on the eastern boundary is ultimately attributed to remote processes: these can be diabatic processes in the equatorial region, or the deepening of stratification in the Southern Ocean.

In section 7 we propose an alternative expression for h , which also takes into account that the time-averaged buoyancy is not vertically homogeneous in the dynamically active region of the EBC: with eddies, the vertical advection of mean buoyancy is balanced by eddy fluxes, which restratify the profile, leading to sloping isopycnals, and locally maintain a region of horizontal buoyancy gradients.

The width of the EBC is illustrated in Fig. 5, where the vertical average of the northward (Fig. 5a) and southward

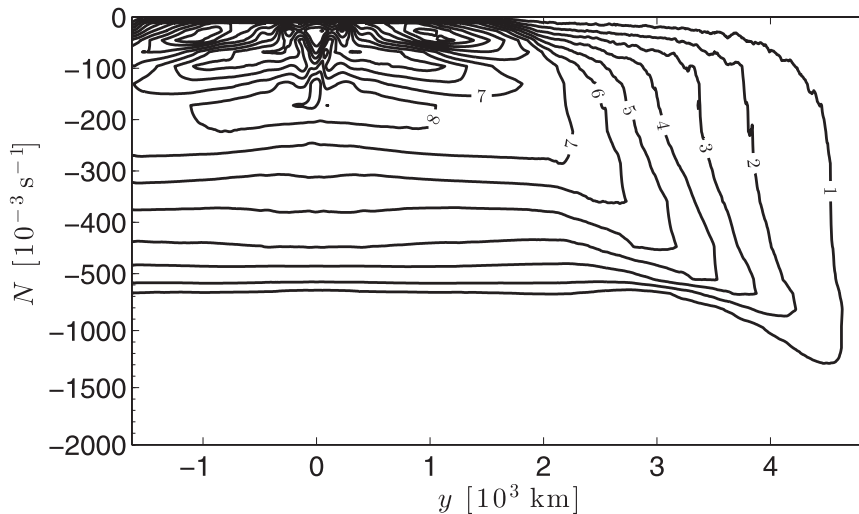


FIG. 4. Time-averaged Brunt–Väisälä frequency, $N \equiv \sqrt{b_z}$, on the eastern boundary contoured as a function of y and z (CI: $1 \times 10^{-3} \text{ s}^{-1}$).

(Fig. 5b) meridional velocity is contoured for the easternmost 100 km of the domain. It is clear from Fig. 5 that the width of the meridional current decreases with latitude. The thick solid line in Fig. 5 also shows the distance from the eastern boundary of the first baroclinic radius calculated using the Wentzel–Kramers–Brillouin (WKB) approximation as in Chelton et al. (1998). The widths of both the equator- and poleward currents follow this estimate of the Rossby radius well. The core of the current shows a weak dependence on latitude; we conjecture that the position of the current core is determined by the no-slip condition, which is satisfied in a side viscous Ekman layer [cf. appendix C in Schloesser et al. (2012)].

The width of the current as shown in Fig. 5 is much larger than the side Ekman layer width, $\sqrt{2\nu/f}$, which is about 500 m, and indeed we find that viscosity is negligible in the EBC, except very close to the solid boundary, where the no-slip condition is applied.¹

While the time-averaged current is apparent, snapshots of the velocity field show a sea of eddies confined near the coast, through which is difficult to discern the sense of propagation of the mean current. This point has been made before (Marchesiello et al. 2003; Todd et al. 2012).² In the following section we show that when eddies are taken into account, the time-mean zonal and vertical flow in buoyancy coordinates is qualitatively different from the flow in level coordinates. In particular,

the net vertical flow in buoyancy coordinates, that is, the diapycnal velocity, is negligible, indicating that the flow is confined to isopycnal surfaces, even near the boundary. In this sense, the EBC is not the downwelling (or upwelling) limb of the zonal (or meridional) overturning circulation, as previously suggested (Marotzke 1997; Spall and Pickart 2001; Pedlosky and Spall 2005; Spall 2010). Instead, the EBC is an adiabatic boundary current, which is part of the interior horizontal circulation. Unlike the interior circulation, eddy fluxes of buoyancy and momentum are essential for its dynamics, as they allow breaking of the geostrophic constraint and the conservation of mean potential vorticity, without diabatic and viscous processes. In this way, the mean buoyancy gradients imposed at the surface can penetrate the water column on the solid boundary, to a depth that depends on the eddy processes.

4. Thickness-weighted average circulation

We illustrate circulation by considering the thickness-weighted averaged (TWA) zonal velocity \hat{u} in buoyancy coordinates (De Szoeke and Bennett 1993; McDougall and McIntosh 1996, 2001; Young 2012). The TWA enables diagnosis of the dynamics and balances in the EBC system, by naturally incorporating the rectified effects of eddy fluxes of buoyancy and momentum. For the detailed derivation and application of the TWA formalism, the reader is referred to Young (2012), whose main results are summarized here.

The TWA of a field θ is defined as

$$\hat{\theta} \equiv \frac{\overline{\sigma\theta}}{\overline{\sigma}}, \quad (5)$$

¹ The viscous and hyperviscous Ekman thicknesses in the subtropical gyre are 500 and 1000 m, respectively.

² Unlike these references, we lack a surface equatorward current because we do not have wind along the coast.

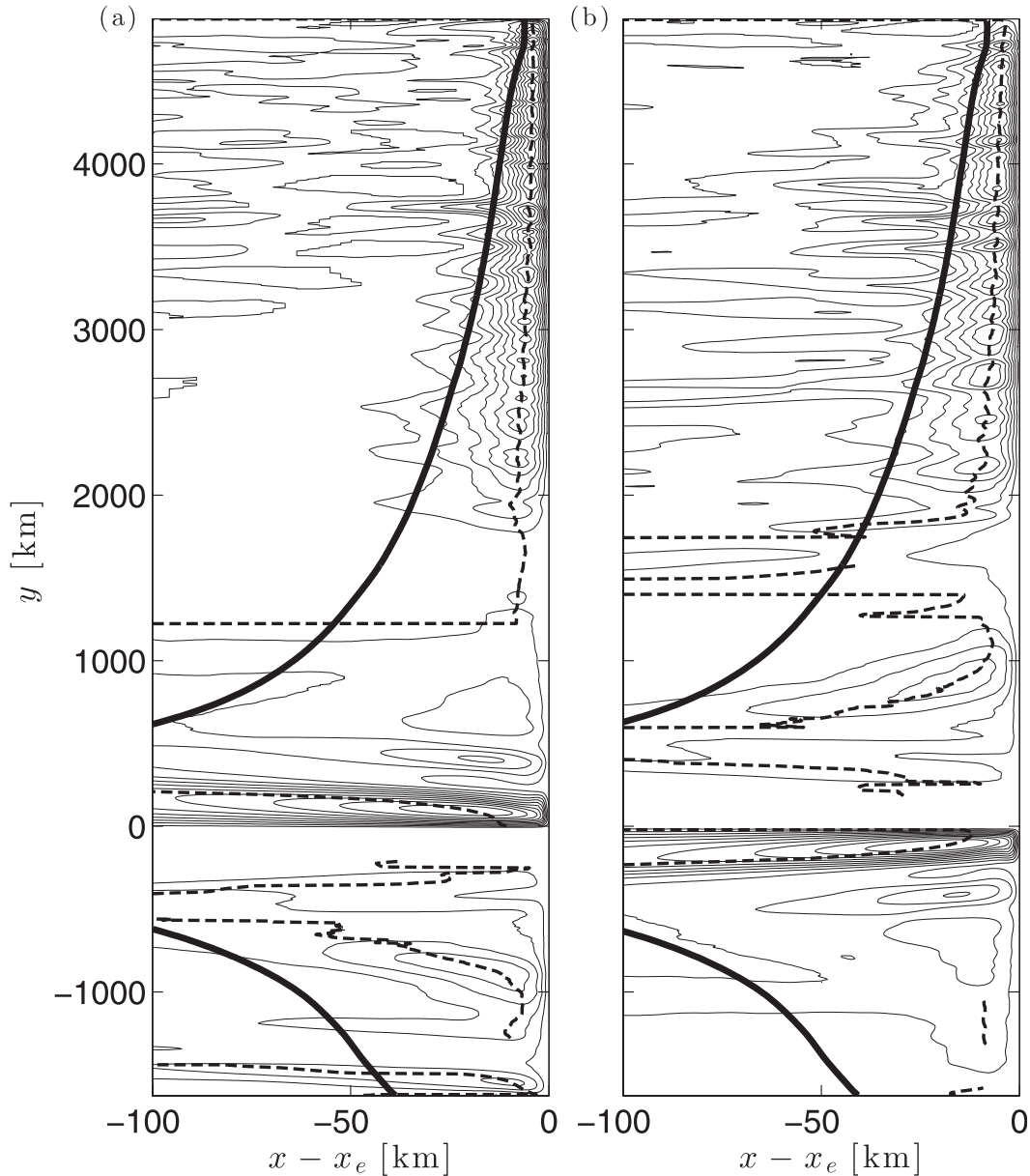


FIG. 5. The vertical average (m s^{-1}) of the (a) northward and (b) southward time-average meridional velocity (contoured in the x - y plane; CI: $6 \times 10^{-3} \text{ m s}^{-1}$). Thick solid line indicates the distance from the eastern boundary of the first baroclinic deformation radius, calculated according to WKB theory. Position of the core of the meridional current is indicated by the dashed line.

where the “thickness weight” σ is defined as

$$\sigma \equiv \zeta_{\tilde{b}}, \tag{6}$$

and the overbar represents the ensemble average at constant b , which we approximate with a time average. Here, ζ is the height of a buoyancy surface b , so that $\sigma = b_z^{-1}$. The symbol \tilde{b} denotes the buoyancy as an independent coordinate, while b denotes buoyancy in

level coordinates, that is, the function $b(x, y, z, t)$. In buoyancy coordinates, the residual velocity is

$$\mathbf{u}^\# = \tilde{u}\bar{\mathbf{e}}_1 + \tilde{v}\bar{\mathbf{e}}_2 + \bar{\sigma}^{-1}(\tilde{\zeta}_i + \tilde{\omega}\tilde{\zeta}_{\tilde{b}})\bar{\mathbf{e}}_3, \tag{7}$$

where derivatives with respect to variables with a tilde are taken at constant b , $\tilde{\omega}$ is the diabatic source (or sink) of buoyancy, and the vectors $\bar{\mathbf{e}}_j$ are defined as

$$\bar{\mathbf{e}}_1 = \mathbf{i} + \bar{\zeta}_x \mathbf{k}, \quad (8)$$

$$\bar{\mathbf{e}}_2 = \mathbf{j} + \bar{\zeta}_y \mathbf{k}, \quad \text{and} \quad (9)$$

$$\bar{\mathbf{e}}_3 = \bar{\sigma} \mathbf{k}, \quad (10)$$

where \mathbf{i} , \mathbf{j} , and \mathbf{k} are the unit vectors in the x , y , and z directions, respectively. The term being multiplied to $\bar{\mathbf{e}}_3$ in (7) defines the diapycnal component of the velocity and the terms being multiplied to $\bar{\mathbf{e}}_1$ and $\bar{\mathbf{e}}_2$ define the horizontal components of the velocity. Notice that the diapycnal term is vertical in the non-orthogonal basis $\bar{\mathbf{e}}$. This decomposition is necessary in order to ensure that $\mathbf{u}^\#$ is nondivergent. In level coordinates, the (incompressible) three-dimensional residual velocity is given by

$$\mathbf{u}^\# = \hat{u} \mathbf{i} + \hat{v} \mathbf{j} + w^\# \mathbf{k}, \quad (11)$$

where the vertical component

$$w^\# \equiv \bar{\zeta}_z + \hat{u} \bar{\zeta}_x + \hat{v} \bar{\zeta}_y + \hat{\omega} \bar{\zeta}_b \quad (12)$$

clearly differs from the diapycnal component, which is the final term in (7).

A useful result of these coordinate and variable transformations is that the average buoyancy and continuity equations combine to give

$$\bar{\sigma}_z + (\hat{u} \bar{\sigma})_x + (\hat{v} \bar{\sigma})_y + (\hat{\omega} \bar{\sigma})_b = 0. \quad (13)$$

This shows that in a steady state (or if the ensemble average is a time average) and for adiabatic flow where $\hat{\omega} = 0$, TWA transport is nondivergent on a buoyancy surface.

With the TWA formalism it is straightforward to show that the dynamics of the EBC are adiabatic. This is best illustrated in Fig. 6 where $\bar{\sigma} \mathbf{u}^\#$ is contoured in buoyancy coordinates at a section located at $y = 3000$ km across the EBC. The thickness-weighted, time-mean velocities following isopycnals include the contribution of the eddy correlation between velocity and isopycnal heights. In this sense, \hat{u} and \hat{v} are “residual” velocities in isopycnal coordinates. It is useful to partition the transport field into a time-mean component, denoted with an overbar (lhs column in Fig. 6), and an eddy contribution (central column in Fig. 6) arising from time-dependent eddies, denoted with a superscript asterisk. In essence, the TWA horizontal transport is written as

$$\mathbf{u}^\# = \nabla \times (\mathbf{k} \times \boldsymbol{\psi}), \quad (14)$$

where $\boldsymbol{\psi} \equiv \psi_1 \mathbf{i} + \psi_2 \mathbf{j}$, is a horizontal vector streamfunction satisfying³

$$\bar{\sigma} \mathbf{u}^\# = -\psi_{1b} \bar{\mathbf{e}}_1 - \psi_{2b} \bar{\mathbf{e}}_2 + (\psi_{1x} + \psi_{2y}) \bar{\mathbf{e}}_3. \quad (15)$$

Note that the third component of the residual transport, given by

$$\bar{\zeta}_z + \bar{\sigma} \hat{\omega} = \psi_{1x} + \psi_{2y}, \quad (16)$$

vanishes for adiabatic, stationary processes. A streamfunction satisfying (14) is

$$\boldsymbol{\psi} = \int_{-H}^0 (\mathbf{u} \mathbf{i} + \mathbf{v} \mathbf{j}) \mathcal{H}[b(x, y, z, t) - \tilde{b}] dz, \quad (17)$$

where H is the depth and \mathcal{H} indicates the Heaviside function, and this is the definition used here. The streamfunction $\boldsymbol{\psi}$ is then decomposed into an Eulerian-mean streamfunction $\boldsymbol{\psi}^\circ$ and an eddy streamfunction $\boldsymbol{\psi}^\star$. The mean and eddy velocities are then calculated taking the curl of the streamfunctions in (18); this ensures that both components of the velocity are divergence free. Specifically, we make the definitions

$$\boldsymbol{\psi}^\circ \equiv \int_{-H}^0 [\bar{u}^z(x, y, z) \mathbf{i} + \bar{v}^z(x, y, z) \mathbf{j}] \mathcal{H}[\bar{b}^z(x, y, z) - \tilde{b}] dz$$

and $\boldsymbol{\psi}^\star \equiv \boldsymbol{\psi} - \boldsymbol{\psi}^\circ,$ (18)

where the overbar and superscript z denote the time mean at constant z . The associated mean and eddy velocities are

$$\mathbf{u}^\circ \equiv \nabla \times (\mathbf{k} \times \boldsymbol{\psi}^\circ) \quad \text{and} \quad \mathbf{u}^\star \equiv \nabla \times (\mathbf{k} \times \boldsymbol{\psi}^\star). \quad (19)$$

In particular, we define the third components of the transports as

$$\bar{\sigma} \sigma^\circ \equiv \psi_{1x}^\circ + \psi_{2y}^\circ \quad \text{and} \quad \bar{\sigma} \sigma^\star \equiv \psi_{1x}^\star + \psi_{2y}^\star. \quad (20)$$

For monotonic \bar{b}^z ,

$$\mathbf{u}^\circ = \frac{1}{\bar{\sigma} \bar{b}_z^z} \bar{\mathbf{u}}^z, \quad (21)$$

so that $\mathbf{u}^\circ = \bar{\mathbf{u}}^z$ in the limit of quasi-level buoyancy surfaces.

³ The curl of a horizontal vector $\mathbf{q} = q_1 \mathbf{i} + q_2 \mathbf{j}$ expressed in the $\bar{\mathbf{e}}$ basis is $\nabla \times \mathbf{q} = \bar{\sigma}^{-1} [-q_{2,b} \bar{\mathbf{e}}_1 + q_{1,b} \bar{\mathbf{e}}_2 + (q_{2,x} - q_{1,y}) \bar{\mathbf{e}}_3]$ [see the appendix in Young (2012)].

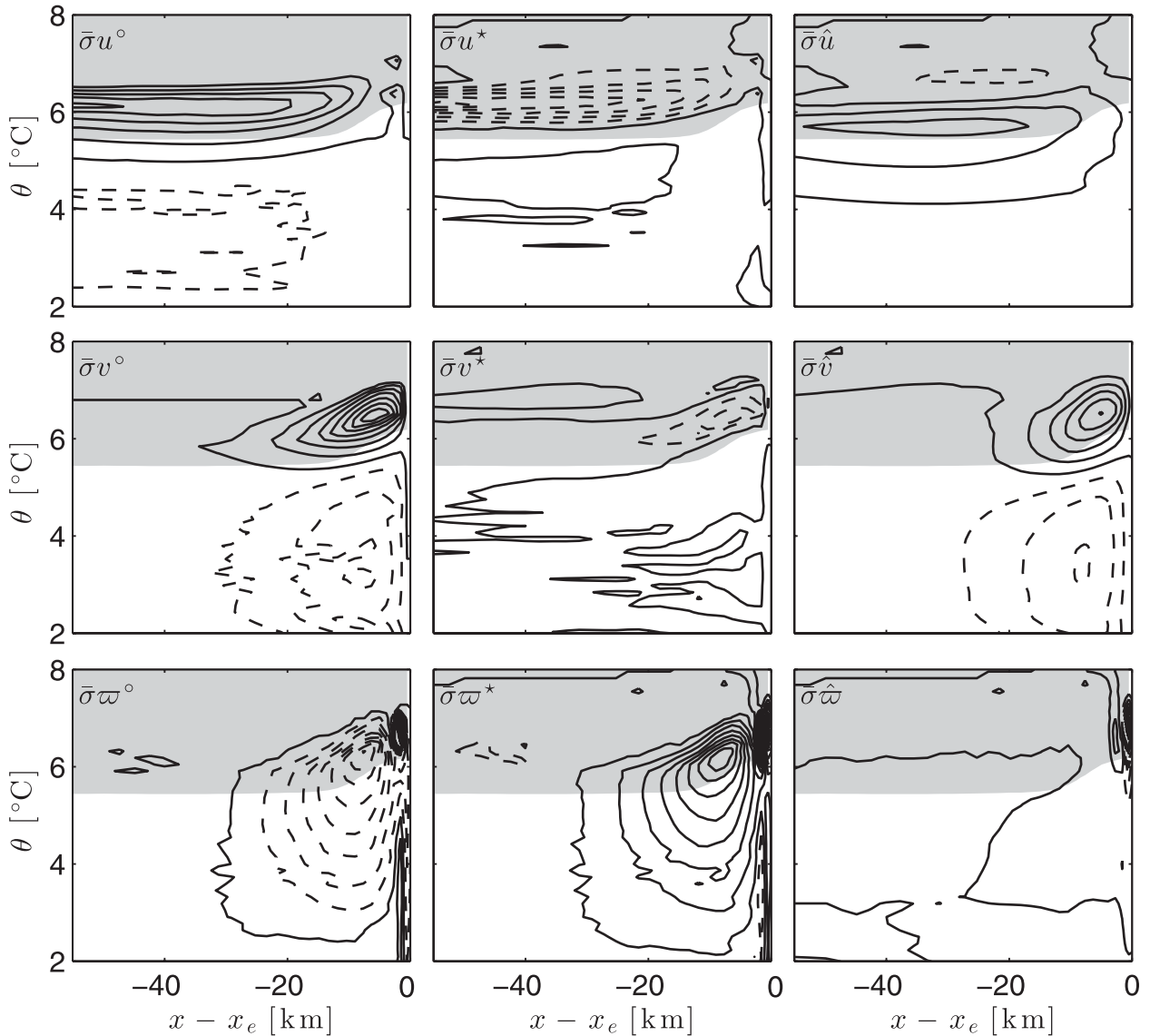


FIG. 6. The three components of $\bar{\sigma}\mathbf{u}^{\#}$ at $y = 3000$ km are shown as a function of \bar{x} and $\bar{\theta}$. Here, (top row, rhs) $\bar{\sigma}\hat{u}$, (middle row, rhs) $\bar{\sigma}\hat{v}$, and (bottom row, rhs) $\bar{\sigma}\hat{w} + \bar{\zeta}_t$ are shown. The lhs and central columns additionally show the contributions of the residual transport from the time-mean and eddy components respectively. The definitions of the fields are given in the text. The CI are 300 m s , 2000 m s , and $2 \times 10^{-5} \text{ m s}^{-1}$ for the top, middle, and bottom rows, respectively; negative contours are dashed. The swath is shaded gray.

Figure 6 shows that there is a substantial cancellation between mean and eddy components in the zonal velocity \hat{u} and an almost complete cancellation in the diapycnal component \hat{w} , indicating that the flow is adiabatic except for the near-surface region. In contrast, there is no appreciable eddy contribution in the meridional velocity \hat{v} , which is almost entirely determined by the mean component. Notice that there is a qualitative difference between u° and \hat{u} : u° changes sign below the diabatic layer (shaded in gray in Fig. 6), suggesting an overturning cell in the x - z plane, while \hat{u} is of a single sign in this region.

The striking cancellation between mean and eddy components in the diapycnal velocity can be understood in terms of more familiar quantities in level coordinates by observing that

$$\psi_{1\bar{x}}^{\circ} + \psi_{2\bar{y}}^{\circ} = \int_{-H}^0 \bar{\mathbf{u}}^z \cdot \nabla \bar{b}^z \delta(\bar{b}^z - \tilde{b}) dz = \frac{\bar{\mathbf{u}}^z \cdot \nabla \bar{b}^z}{\bar{b}_z^z}, \quad (22)$$

where the second equality is only valid if \bar{b}_z^z is monotonic. For the eddy-component, in the limit $\bar{b}^{2z} \rightarrow 0$, we can make the approximation

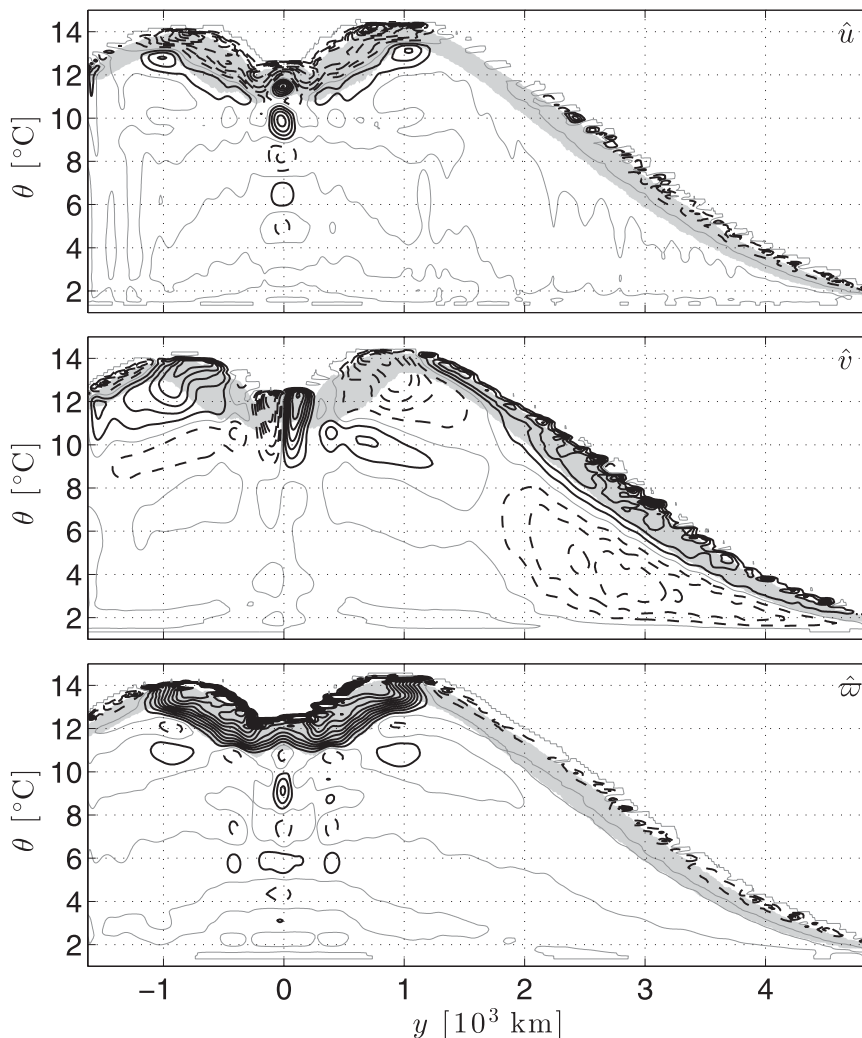


FIG. 7. The velocity 10 km west of the eastern boundary is shown as a function of y and b . Here, (top) \hat{u} , (middle) \hat{v} , and (bottom) \hat{w} are shown. The CI are 1 cm s^{-1} , 4 cm s^{-1} , and $5 \times 10^{-10} \text{ m s}^{-3}$ for the top, middle, and bottom panels, respectively; negative contours are dashed and the zero contour is thin and gray. The swath is shaded gray.

$$\psi_{1\bar{x}}^{\star} + \psi_{2\bar{y}}^{\star} = \int_{-H}^0 \frac{\overline{\mathbf{u}' \cdot \nabla b'^z} \delta(\bar{b}^z - \tilde{b}) dz}{\bar{b}_z^z} \quad (23)$$

The cancellation of the vertical buoyancy transport in the EBC has been noted before (Spall 2010; Colas et al. 2013), but is especially clear in the TWA framework, which does not require linearization around a mean stratification.

The only region where diabatic effects are important is within about 1000 km of the equator, where the interior circulation is confined near the surface by the strong Ekman suction associated with the tropical gyre. Because of wind-driven upwelling, the isopycnals are

drawn toward the surface, where diabatic effects are important. Thus, within 1000 km of the equator, the bulk of the EBC occurs in a surface diabatic region. This is illustrated in Fig. 7, which shows \hat{v} (top panel) and \hat{w} (lower panel) as a function of θ and y along a section located 10 km west of the eastern boundary. Within 1000 km of the equator \hat{w} is large and positive for most of the depth occupied by the EBC, and $(\overline{\sigma\hat{w}})_{\bar{b}}$ almost singlehandedly balances $(\overline{\sigma\hat{u}})_{\bar{x}}$ (not shown). The region containing the diabatic vertical and zonal circulation ($y < 1000$ km) has a “reversed” meridional EBC, equatorward at the surface and poleward below. In the region $1000 < y < 1800$ there is a complex baroclinic current with several sign reversals in

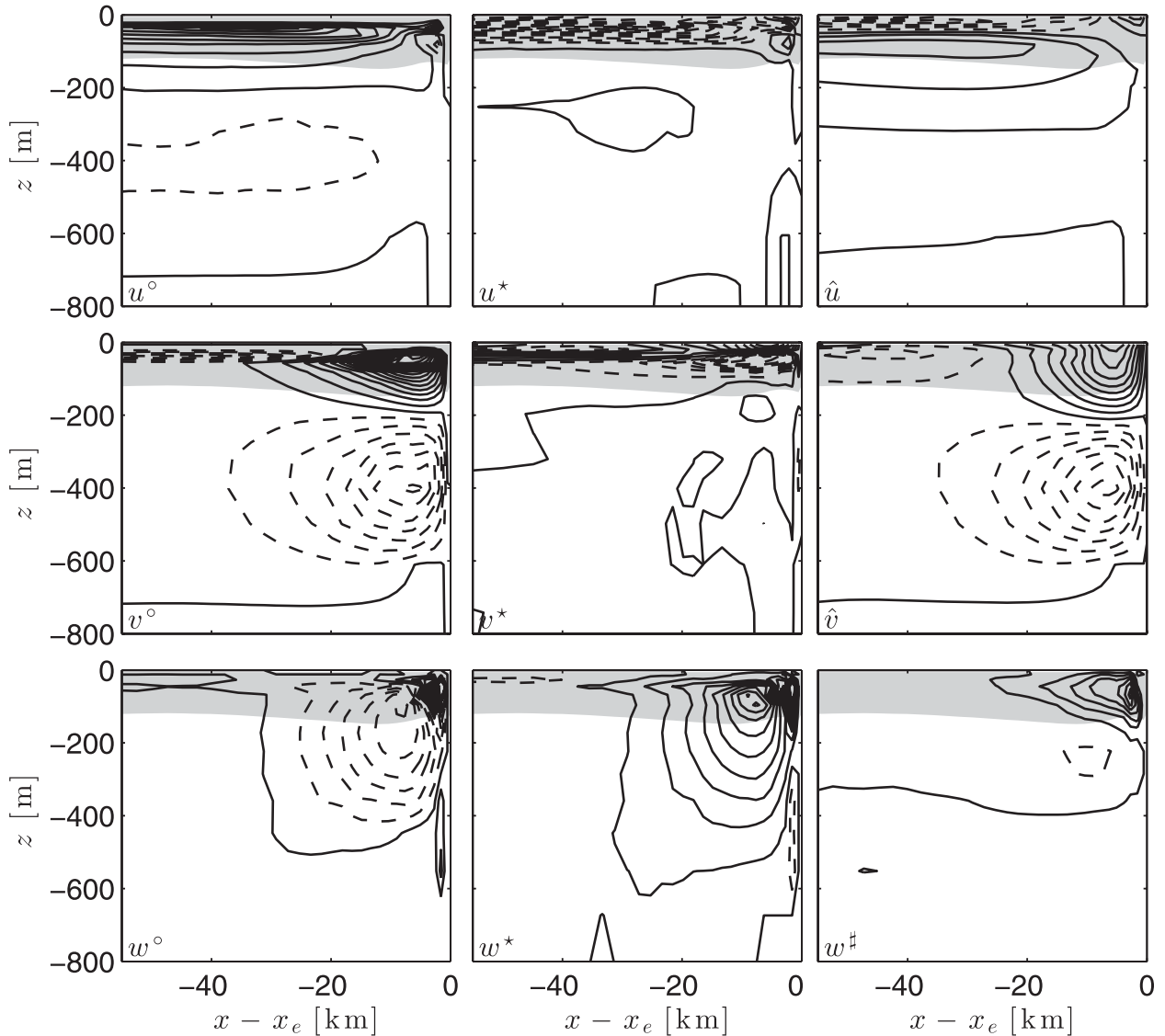


FIG. 8. The three components of $\mathbf{u}^\#$, defined in (11), at $y = 3000$ km are shown as a function of x and z . Here, (top row, rhs) \hat{u} , (middle row, rhs) \hat{v} , and (bottom row, rhs) $w^\#$ are shown. The lhs and central columns additionally show the contributions of the residual velocity from the time-mean and eddy components, respectively. The definitions of the fields are given in the text. The CI are 0.5 cm s^{-1} , 2 cm s^{-1} , and $2 \times 10^{-5} \text{ m s}^{-1}$ for the top, middle, and bottom rows, respectively; negative contours are dashed. The swash is shaded gray.

the vertical, both in the meridional and in the diapycnal velocity components (cf. the middle and bottom panels of Fig. 7). In this transition region, all three components of the velocity contribute to the buoyancy balance (13).

We conclude that the EBC is not associated with an overturning circulation as suggested by previous authors except in the tropics; instead the EBC is part of the along-isopycnal circulation, which occurs quasi-adiabatically once the flow is subducted. To appreciate the two-dimensional character of the flow, it is necessary to go into buoyancy coordinates and perform the appropriate thickness-weighted time

average to evaluate the residual circulation; the TWA formalism is a useful method for this purpose. We note that the vertical component of the TWA velocity in height coordinates does not vanish, as illustrated in Fig. 8. This is because the along-isopycnal velocity has a projection on the vertical, even when the flow is adiabatic. In the EBC, sloping isopycnals depart substantially from the horizontal, and thus $w^\#$ is not a good approximation for the diapycnal velocity \hat{w} . It is interesting to note that, at this particular section, $w^\#$ is positive near the surface, even though the time-averaged vertical velocity \bar{w} is negative in that region.

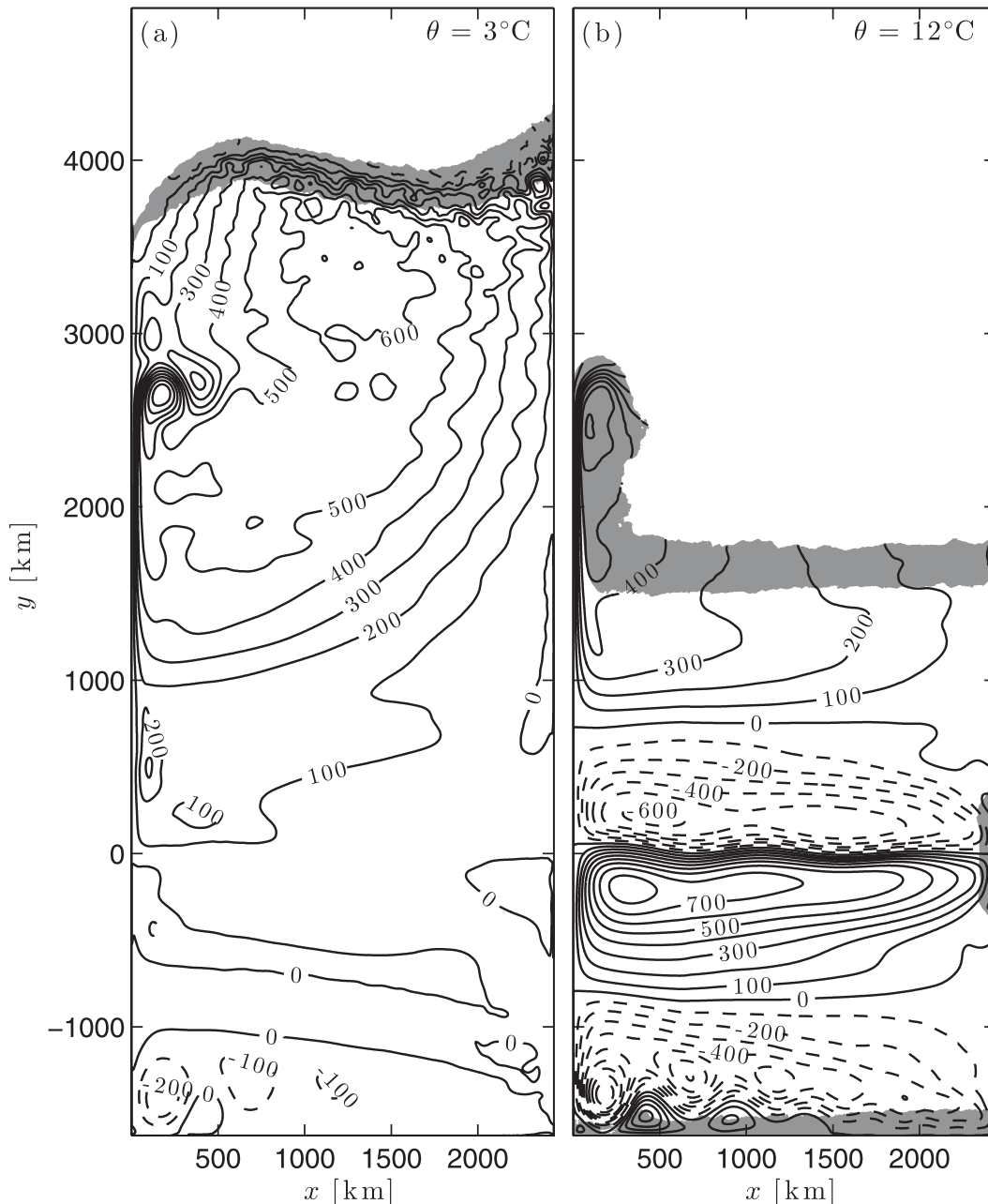


FIG. 9. Streamlines, defined in (24), contoured on the x - y plane for (a) the buoyancy level $b = 0.006 \text{ m s}^{-2}$ corresponding to the 3°C isotherm. Large-scale circulation is anticyclonic except for a small cyclonic gyrelet in the northeastern corner, where the poleward EBC is found. Streamlines hug the eastern boundary closely, giving rise to the equatorward component of the EBC, along the high PV region. (b) The Ψ on the buoyancy level $b = 0.024 \text{ m s}^{-2}$ corresponding to the 12°C isotherm. In the tropics, there are cyclonic circulations, associated with the tropical wind-driven gyres, which are also intensified to the east and west, giving rise to the surface poleward branch of the tropical EBC.

5. The circulation on isopycnals

To understand the vertical and horizontal scales of the EBC, we analyze the time-averaged potential vorticity

dynamics on buoyancy surfaces. Because of the two-dimensional character of the TWA circulation, the flow is best visualized using the horizontal streamfunction Ψ , associated with the approximately horizontally

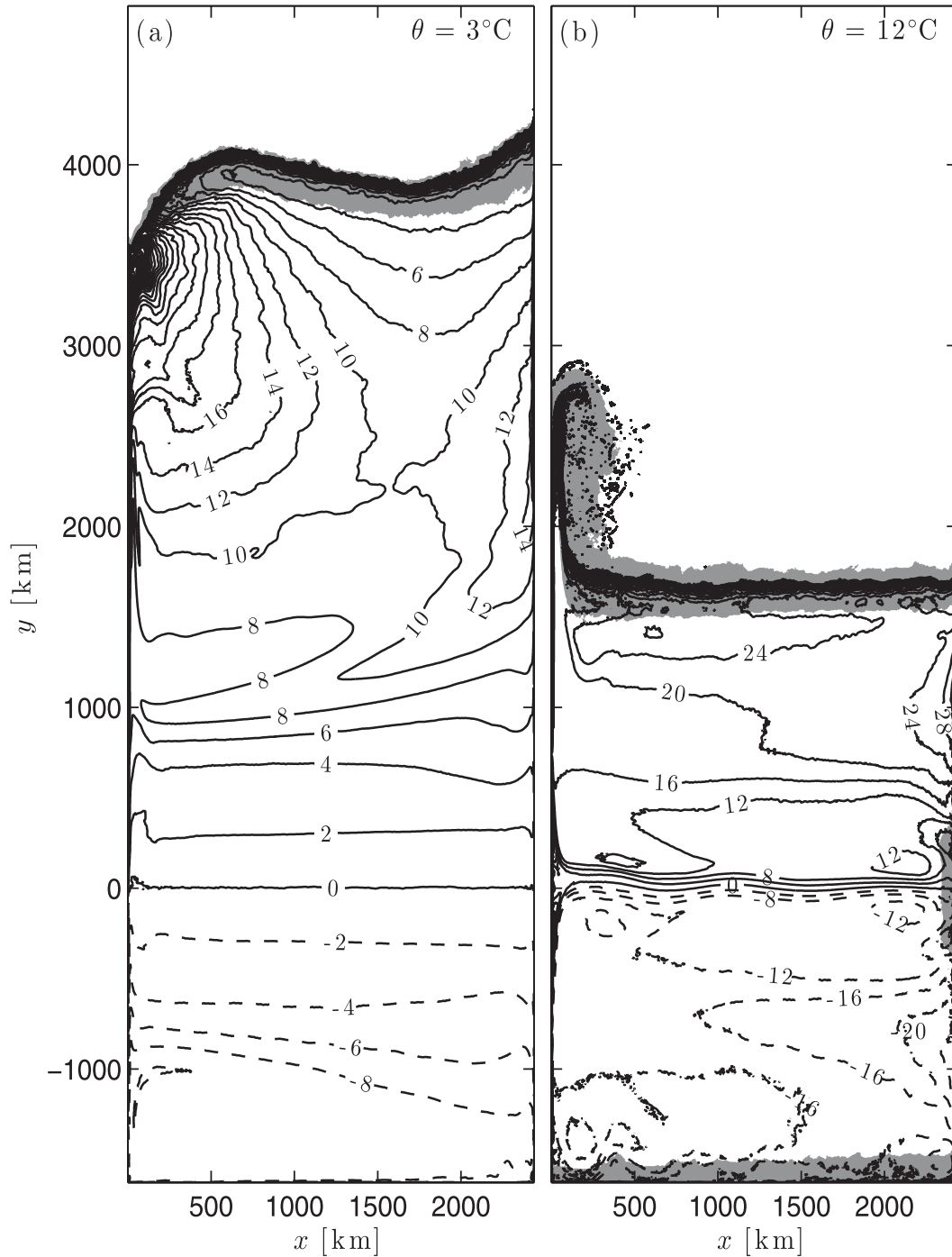


FIG. 10. (a) Averaged PV Π^2 defined in (25), contoured in the x - y plane for the buoyancy level $b = 0.006 \text{ m s}^{-2}$, corresponding to the 3°C isotherm. The swash, defined as the region where the isopycnal is in contact with the surface more than 1% of the time, is gray in both panels. Notice the low PV tongue emanating from the center of the swash, the maximum of PV emanating from the eastern boundary, and the homogenized region in between. (b) Averaged PV for the buoyancy level 0.024 m s^{-2} , corresponding to the 12°C isotherm. Notice the high PV tongue emanating from the center of the swash (as predicted by thermocline theory), the max PV emanating from the eastern boundary, and the homogenized region in between. The CI is $2 \times 10^{-10} \text{ s}^{-3}$ for (a) and $4 \times 10^{-10} \text{ s}^{-3}$ for (b).

nondivergent transport $\overline{\sigma\hat{\mathbf{u}}}$ on isopycnal surfaces, such that

$$\Psi_{\hat{y}} = -\overline{\sigma\hat{u}} \quad \text{and} \quad \Psi_{\hat{x}} = \overline{\sigma\hat{v}}. \quad (24)$$

The Ertel TWA potential vorticity is given by (Young 2012)

$$\Pi^{\#} \equiv \frac{f + \hat{v}_{\hat{x}} - \hat{u}_{\hat{y}}}{\overline{\sigma}}. \quad (25)$$

For all the isopycnals examined, we find that the relative vorticity term $\hat{v}_{\hat{x}} - \hat{u}_{\hat{y}}$ is negligible relative to f except very close to the equator and the western boundary current, so in the following we will limit our discussion to the averaged large-scale vorticity $f/\overline{\sigma}$.

Figures 9 and 10 show Ψ and $\Pi^{\#}$ on two isopycnals that are characteristic of the tropical/subtropical and subpolar circulation, respectively. Because the flow is not exactly two-dimensional in the diabatic “swash” where the isopycnal is in contact for a certain amount of time with the surface (gray shading in Fig. 10), the velocity also has a small divergent component. Therefore, it is not possible to calculate Ψ by simple integration of the transport $\overline{\sigma\hat{\mathbf{u}}}$. Instead, Ψ is calculated by inverting the two-dimensional Poisson equation

$$\nabla^2\Psi = (\overline{\sigma\hat{v}})_{\hat{x}} - (\overline{\sigma\hat{u}})_{\hat{y}}, \quad (26)$$

with conditions $\Psi = 0$ on the solid boundaries. The horizontal velocity associated with the divergent part of the flow (not shown) is smaller than $\overline{\sigma\hat{\mathbf{u}}}$, except in some localized regions in the swash, where the two components are comparable.

On every isopycnal north of about $y = 1000$ km, the circulation is anticyclonic except for a small cell of cyclonic flow in the northeastern corner, near the intersection of the swash with the eastern boundary; this region corresponds to the poleward surface component of the EBC system.

The anticyclonic circulation is closed by a boundary current at the eastern boundary, which lacks a barotropic component and by a stronger western boundary current with a sizeable barotropic current. The streamlines run close and parallel to the eastern boundary until about $y = 1800$ km, which represents the northern boundary of the tropical region where the meridional current is reversed. Thus, the equatorward part of the EBC in the subpolar and subtropical regions is part of the interior baroclinic circulation, except that, near the eastern boundary, mean streamlines are not constrained to flow along mean potential vorticity contours because

of the eddy fluxes terms (cf. Fig. 9a and Fig. 10a). The eddy fluxes of buoyancy and momentum allow flow along and across the potential vorticity (PV) contours that intersect the eastern boundary, breaking the constraint of the zero buoyancy gradient along the eastern wall. The sense of circulation near the boundary is in the same sense as the interior circulation (anticyclonic), but the encounter with the coast accelerates the meridional velocity while decelerating the zonal flow. As demonstrated in the next section, the EBC arises in a boundary layer where the TWA velocity normal to the eastern boundary is brought to zero in a region of finite depth, contrary to the assumption of laminar thermocline theories. The meridional component of the EBC has a zero vertical average, consistent with the Sverdrup constraint on the barotropic flow. This constraint is achieved by reversing the current in a region which, in isopycnal coordinates, is limited in latitude and confined to the swash.

Conversely, the tropical cyclonic circulation is associated with a cyclonic circulation which is accompanied by a poleward EBC, characterized by a decreased spacing of the streamlines as the eastern boundary is approached (cf. Fig. 9b).

6. The potential vorticity balance

On all isopycnals there is a clear source of high potential vorticity emanating from the eastern boundary—this is caused by the smoothed jump in buoyancy that separates the “bowl” containing horizontal gradients of $\bar{\zeta}$ from the resting region below, in which $\bar{\zeta}$ is a function of b only. On the eastern wall, the boundary between the two regions corresponds to the depth $z = -h(y)$ discussed in section 3 (cf. Fig. 3). The high potential vorticity corresponds to the maximum in stratification on the eastern boundary (cf. Fig. 4). This maximum is “diffused” in the interior by eddy fluxes of thickness and momentum while being advected along the streamlines Ψ (Colin de Verdière 1989; Sumata and Kubokawa 2001).

Because the average relative vorticity is negligible relative to f , it is useful to consider the large-scale limit of the potential vorticity balance, where time dependence and inertia are neglected, while keeping the eddy fluxes of momentum and thickness.

At the large-scale limit, the thickness-averaged momentum equations⁴ become (Young 2012)

⁴ The viscous term in the meridional equation does not appear in Young (2012), and it is here approximated with $\nabla^4\bar{v}$, where $\nabla^4 = \partial_{xxxx} + 2\partial_{xxyy} + \partial_{yyyy}$.

$$-f\hat{v} + \overline{m}_x + \nabla \cdot \mathbf{E}^u = \hat{\lambda} \quad \text{and} \quad (27)$$

$$f\hat{u} + \overline{m}_y + \nabla \cdot \mathbf{E}^v = \hat{y} - \nu_4 \nabla^4 \bar{v}. \quad (28)$$

Here, $(\mathcal{X}, \mathcal{Y})$ is the mechanical forcing and friction, $m = p - b\zeta$ is the Montgomery potential, and the Eliassen-Palm (EP) vectors \mathbf{E}^u and \mathbf{E}^v are given by

$$\mathbf{E}^u \equiv \mathbf{J}^u + \bar{\sigma}^{-1} \left[(1/2)\overline{\zeta'^2} \mathbf{e}_1 + \overline{\zeta' m'_x} \mathbf{e}_3 \right] \quad \text{and} \quad (29)$$

$$\mathbf{E}^v \equiv \mathbf{J}^v + \bar{\sigma}^{-1} \left[(1/2)\overline{\zeta'^2} \mathbf{e}_2 + \overline{\zeta' m'_y} \mathbf{e}_3 \right]. \quad (30)$$

The fluxes \mathbf{J}^u and \mathbf{J}^v are given by

$$\mathbf{J}^c \equiv u'' \widehat{c''} \mathbf{e}_1 + v'' \widehat{c''} \mathbf{e}_2 + \overline{\omega'' c''} \mathbf{e}_3, \quad (31)$$

where $c'' \equiv c - \hat{c}$ represents departures from the TWA, while the departures from the unweighted average are given by $c' \equiv c - \bar{c}$. Notice, that if the EP vectors are given on the \mathbf{e}_i basis, for example, $\mathbf{E} = E^1 \mathbf{e}_1 + E^2 \mathbf{e}_2 + E^3 \mathbf{e}_3$, then the divergence is given by

$$\nabla \cdot \mathbf{E} = \bar{\sigma}^{-1} (\overline{\sigma E^1})_{\hat{x}} + \bar{\sigma}^{-1} (\overline{\sigma E^2})_{\hat{y}} + \bar{\sigma}^{-1} (\overline{\sigma E^3})_{\hat{b}}. \quad (32)$$

Given this definition, it is convenient to multiply the momentum equations by $\bar{\sigma}$ and cross differentiate to get the following form of the large-scale PV balance:

$$\begin{aligned} & f[(\overline{\sigma \hat{u}})_{\hat{x}} + (\overline{\sigma \hat{v}})_{\hat{y}}] + \beta \overline{\sigma \hat{v}} + \overline{\sigma_x \bar{m}_y} - \overline{\sigma_y \bar{m}_x} \\ &= (\overline{\sigma \nabla \cdot \mathbf{E}^u} - \overline{\sigma \hat{\lambda}})_{\hat{y}} - (\overline{\sigma \nabla \cdot \mathbf{E}^v} - \overline{\sigma \hat{y}} + \nu_4 \overline{\sigma \nabla^4 \bar{v}})_{\hat{x}}. \end{aligned} \quad (33)$$

Using (13) to eliminate the first term on the lhs of (33), (27) to eliminate the second term on the lhs, and dividing by f , we obtain

$$\begin{aligned} & -\overline{\sigma_{\hat{t}}} - (\overline{\sigma \hat{\omega}})_{\hat{b}} + \overline{m}_y (\overline{\sigma/f})_{\hat{x}} - \overline{m}_x (\overline{\sigma/f})_{\hat{y}} \\ &= \left(\frac{\overline{\sigma \nabla \cdot \mathbf{E}^u}}{f} - \overline{\sigma \hat{\lambda}} \right)_{\hat{y}} - \left(\frac{\overline{\sigma \nabla \cdot \mathbf{E}^v} - \overline{\sigma \hat{y}} + \nu_4 \overline{\sigma \nabla^4 \bar{v}}}{f} \right)_{\hat{x}}. \end{aligned} \quad (34)$$

It is clear that even in statistical steady state, for adiabatic and inviscid conditions, and below the directly wind-forced layer (so that $\hat{\lambda} = \hat{y} = 0$), the large-scale PV is not conserved following the average Montgomery potential \bar{m} because of the eddy fluxes contained in the divergence of the EP vectors \mathbf{E}^u and \mathbf{E}^v .

Near the eastern boundary, we can ignore the wind stress curl and we can neglect $(\overline{\sigma \nabla \cdot \mathbf{E}^u}/f)_{\hat{y}}$ relative to

$(\overline{\sigma \nabla \cdot \mathbf{E}^v}/f)_{\hat{x}}$. Furthermore, we notice that $\nabla \cdot (\mathbf{E}^v - \mathbf{J}^v) = \overline{\sigma' m'_y}$, where the hydrostatic approximation, $m_b = -\zeta$, and the definition $\sigma \equiv \zeta_b$ have been used. Finally, making the boundary layer simplification $\mathbf{J}^v \approx \widehat{u'' v''} \mathbf{e}_1$, we can approximate the rhs of (34) with

$$\begin{aligned} & \left(\frac{\overline{\sigma \nabla \cdot \mathbf{E}^u}}{f} \right)_{\hat{y}} - \left(\frac{\overline{\sigma \nabla \cdot \mathbf{E}^v}}{f} + \nu_4 \overline{\sigma \nabla^4 \bar{v}} \right)_{\hat{x}} \\ & \approx - \left(\frac{\overline{\sigma' m'_y}}{f} \right)_{\hat{x}} - \left[\frac{(\overline{\sigma u'' v''})_{\hat{x}} + \nu_4 \overline{\sigma v_{\hat{x}\hat{x}\hat{x}\hat{x}}}}{f} \right]_{\hat{x}}. \end{aligned} \quad (35)$$

The approximation (35) leads to the following dominant balance in the PV (34):

$$\begin{aligned} & \overline{m}_y (\overline{\sigma/f})_{\hat{x}} - \overline{m}_x (\overline{\sigma/f})_{\hat{y}} \\ & \approx - \left(\frac{\overline{\sigma' m'_y}}{f} \right)_{\hat{x}} - \left[\frac{(\overline{\sigma u'' v''})_{\hat{x}} + \nu_4 \overline{\sigma v_{\hat{x}\hat{x}\hat{x}\hat{x}}}}{f} \right]_{\hat{x}}. \end{aligned} \quad (36)$$

In (36) we have included the viscous term, although it becomes important only in a subregion of the EBC very close to the solid wall. The terms in the dominant balance (36) are shown in Figs. 11, 12, and 13 at a section located at $y = 3005$ km, which is representative of other latitudes in the subtropical and subpolar regions. The dominant balance (36) should be compared with that proposed by Cessi and Wolfe (2009a) and Cessi et al. (2010). In those references, the eddies are parameterized and the quasigeostrophic approximation is made, resulting in the PV balance⁵

$$\beta \bar{v} = \left[-(\overline{u'b'})_x + \frac{\kappa_v \bar{b}_{zz}}{\bar{b}_z} \right]_z. \quad (37)$$

The PV balance (36) differs from (37) in several substantial respects: first, the advection of PV by the mean flow is important in (36), while the advection of the planetary component, retained in (37), is not; second, the eddy momentum flux is as important as the eddy flux of thickness (or buoyancy); and finally, diapycnal diffusion is negligible. The only common term between (36) and (37) is the eddy flux of buoyancy. The next section details how these differences lead to qualitatively different horizontal and vertical scales of the EBC.

The two terms on the lhs of (36) (the mean advection of mean PV) are individually of the same order of

⁵ In the quasigeostrophic approximation used by Cessi and Wolfe (2009a) and Cessi et al. (2010), the average at constant z ($\bar{\cdot}$) and the TWA ($\hat{\cdot}$) coincide, so there is only one time average ($\bar{\cdot}$).

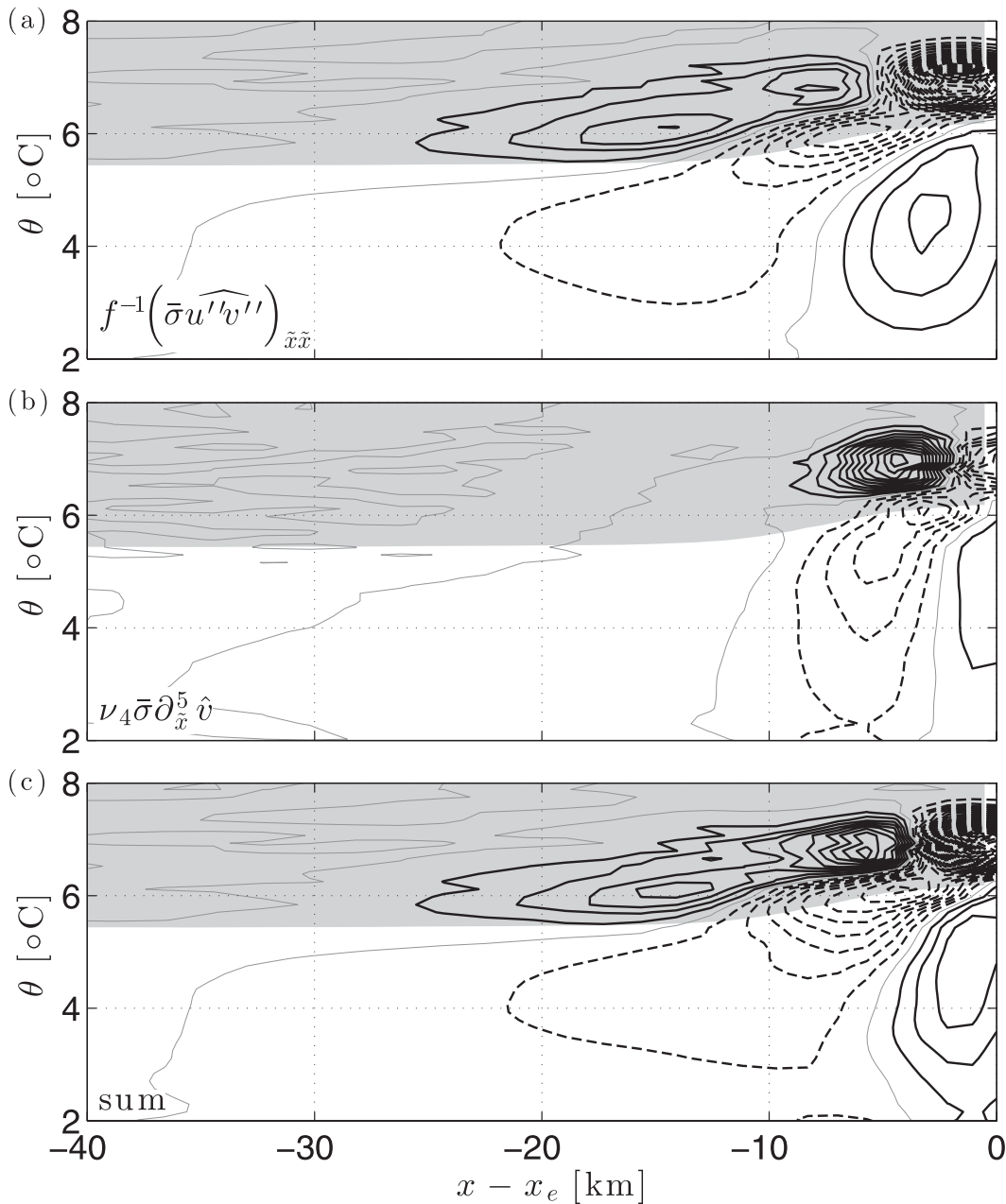


FIG. 11. The terms (a) $(\overline{\sigma u'v'})_{\tilde{x}\tilde{x}}/f$, (b) $\nu_4 \hat{v}_{xxxxx}$, and (c) their sum near the eastern boundary are shown as a function of x and θ at the nominal latitude $y = 3005$ km (all fields are also averaged in y over a 160-km swath). The CI is 0.01 s; negative contours are dashed and the zero contour is thin and gray. The swath is shaded gray.

magnitude as the terms on the rhs, but they add up to a small residual (cf. Fig. 12c with Figs. 11c and 13) so the dominant PV balance is

$$\left(\frac{\overline{\sigma' m'_y}}{f}\right)_{\tilde{x}} + \left[\frac{(\overline{\sigma u'v'})_{\tilde{x}} + \nu_4 \overline{\sigma} \hat{v}_{xxxxx}}{f}\right]_{\tilde{x}} \approx 0. \quad (38)$$

To make further progress, it is necessary to relate the eddy fluxes of buoyancy and momentum to the mean

quantities. Figure 14 shows the term $(\overline{\sigma u'v'})_{\tilde{x}}$, which should be compared with the middle row, rhs of Fig. 6, which shows $\overline{\sigma \hat{v}}$ at the same location. The two quantities are remarkably related and we can thus make the approximation

$$(\overline{\sigma u'v'})_{\tilde{x}} = \mu^2 \overline{\sigma \hat{v}}, \quad (39)$$

where μ^2 is a positive quantity. The point is that the divergence of the eddy flux acts like a drag on the

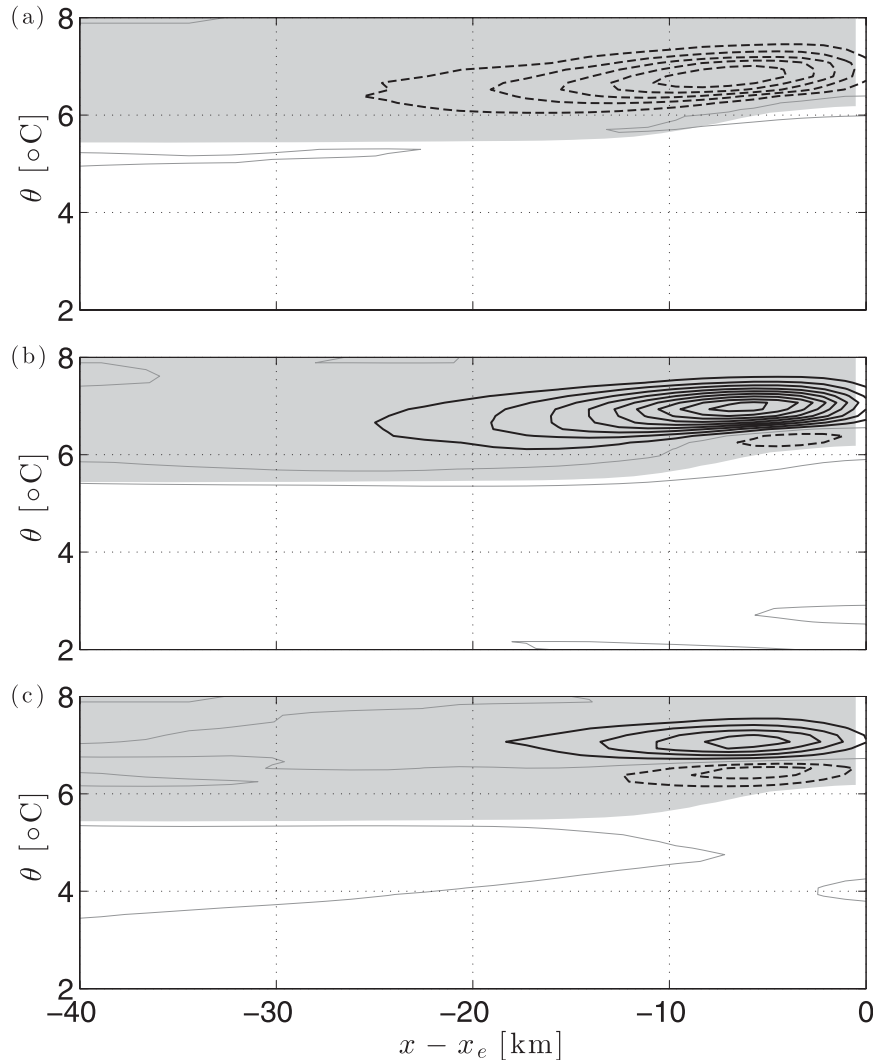


FIG. 12. The terms (a) $\overline{m}_y(\overline{\sigma}/f)_{\bar{x}}$, (b) $-\overline{m}_x(\overline{\sigma}/f)_{\bar{y}}$, and (c) their sum near the eastern boundary are shown as a function of x and θ at the nominal latitude $y = 3005$ km (all fields are also averaged in y over a 160-km swath). The CI is 0.01 s; negative contours are dashed and the zero contour is thin and gray. The swath is shaded gray.

residual meridional velocity. Using this parameterization in (38), we find that there is a vorticity drag (caused by Reynolds stress divergence), which balances the divergence of the eddy form stress term $(\overline{\sigma' m'_y}/f)_{\bar{x}}$.

Assuming that the eddies are geostrophic, then

$$\left(\frac{\overline{\sigma' m'_y}}{f}\right)_{\bar{x}} \approx -(\overline{\sigma' u'})_{\bar{x}}. \tag{40}$$

We now assume that $\overline{\sigma' u'}$ approximately coincides with $\overline{\sigma u^*}$, the eddy component of the residual zonal transport shown in Fig. 6, and defined through (18). Using the definitions in (20), remembering that the eddy

component of the residual transport is divergence free, and noticing that $\overline{\sigma v^*}$ is negligible, we have

$$-(\overline{\sigma' u'})_{\bar{x}} \approx (\overline{\sigma w^*})_{\bar{y}}. \tag{41}$$

Because of the adiabatic nature of the residual flow, we have

$$(\overline{\sigma w^*})_{\bar{y}} = -(\overline{\sigma \overline{w}})_{\bar{y}}. \tag{42}$$

Inserting this result together with (41) and (39) on the rhs of (38), and omitting the viscous term, we have

$$(\overline{\sigma \overline{w}})_{\bar{y}} \approx \frac{\mu^2 \overline{\sigma \hat{v}}_{\bar{x}}}{f}. \tag{43}$$

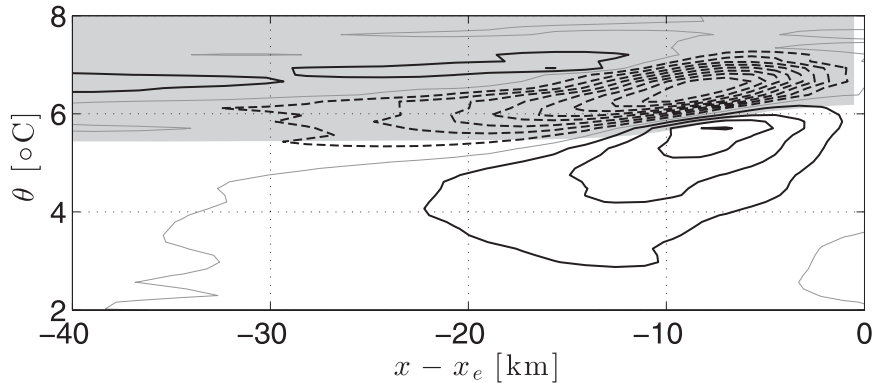


FIG. 13. The term $(\overline{\sigma^l m^l / f})_{\tilde{x}}$ near the eastern boundary is shown as a function of x and θ at the nominal latitude $y = 3005$ km (the field is also averaged in y over a 160-km swath). The CI is 0.01 s; negative contours are dashed and the zero contour is thin and gray. The swash is shaded gray.

In other words, the vortex stretching due to the mean downwelling, mediated by eddy processes, balances the drag caused by Reynolds stress divergence, and this supports a meridional current \hat{v} . Because the current decays toward the west, $\hat{v}_{\tilde{x}}$ has the same structure as \hat{v} . Therefore, (43) illustrates that the mean downwelling shown in Fig. 6 leads to a baroclinic current that is positive in the upper half of the downwelling region and negative in the lower half. The balance in (43) also guarantees that the vertically integrated $\mu^2 \hat{v}$ vanishes. Integrating (43) in \tilde{b} between the range of mean buoyancies found at each horizontal position, the lhs vanishes. Thus we have

$$0 = \int_{b_{\min}}^{b_{\max}} \mu^2 \overline{\sigma} \hat{v}_{\tilde{x}} db = \int_{-h}^0 \mu^2 \hat{v}_{\tilde{x}} dz, \quad (44)$$

where we have used the definition (6) to change the variables from b to z .

Retreating back to the momentum equations, the approximate PV budget (38) corresponds to the following

semigeostrophic balance in the momentum equations (neglecting the viscous term, which matters in a small subregion):

$$-f \hat{v} \approx -\overline{m}_{\tilde{x}} \quad \text{and} \quad (45)$$

$$f \hat{u} \approx -\overline{m}_{\tilde{y}} - \overline{\sigma}^{-1} \overline{\sigma^l m^l}_{\tilde{y}} - \overline{\sigma}^{-1} (\overline{\sigma u'' v''})_{\tilde{x}}. \quad (46)$$

Thus, the “effective boundary condition” of no normal flow on the eastern boundary requires the rhs of (46) to vanish, and this differs from the boundary condition of Cessi et al. (2010) by the divergence of the eddy flux of momentum. As illustrated in the following section, this term is essential in determining the horizontal scale of the EBC.

7. The vertical and horizontal scales of the EBC

To determine the scaling of the EBC in the adiabatic regime, it is useful to make a local geostrophic approximation (40), which, although not quantitatively accurate,

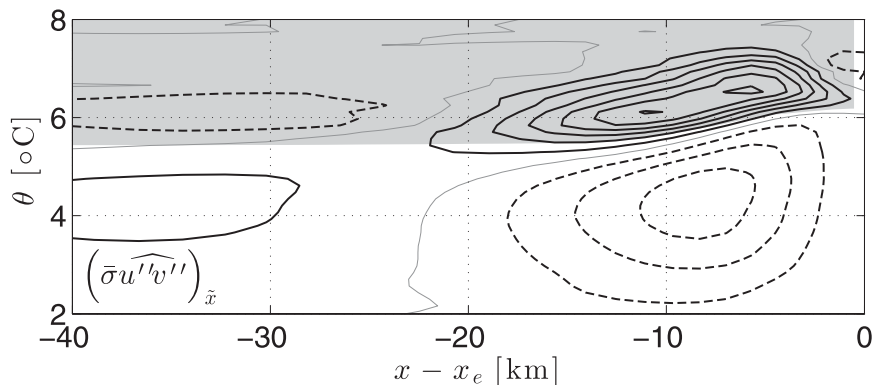


FIG. 14. The term $(\overline{\sigma u'' v''})_{\tilde{x}}$ is shown. Negative contours are dashed and the zero contour is thin and gray. The swash is shaded gray.

allows a better understanding of the dynamics and makes contact with previous theories. This approximation leads to the scaling

$$-(\overline{\sigma' m'_y / f})_{\bar{x}} \sim O(f \overline{\sigma^2} u' v' / h^2), \tag{47}$$

where we have used thermal wind balance ($\sigma'_x \sim f v'_{bb}$) and the scaling $\partial_b \sim h^{-1} \overline{\sigma}$, with h the typical depth of the current.⁶

If we equate the order of magnitude thus found with that of the last term on the rhs of (36), that is,

$$\left[\frac{(\overline{\sigma u' v'})_{\bar{x}}}{f} \right] \sim O(\overline{\sigma} u' v' / f \ell^2), \tag{48}$$

we find that the width of the current ℓ must satisfy

$$\ell \sim \frac{h}{f \sqrt{\overline{\sigma}}}, \tag{49}$$

that is, the width of the current is the baroclinic deformation radius. This scaling is in agreement with the diagnostic shown in Fig. 5, which successfully compares the width of the EBC to the baroclinic deformation radius in the WKB approximation.

It might be surprising that the width of the mean meridional current is on the same scale as the eddies: examination of snapshots of the velocity shows that indeed the mean current is on the same scale as the eddies, which, while alternating in sign, are preferentially of one sign. This property is also observed in the analysis of the California Current system of Todd et al. (2012). The lack of scale separation between eddies and mean does not lend confidence in a mean theory that approximates the eddy fluxes with down-gradient diffusion of the mean quantities.

Despite this premise, and solely to make some progress in the determination of the scales ℓ and h , we shift our ignorance of the eddy statistics in terms of an eddy diffusivity κ , such that

$$(\overline{\sigma' u'}) = -\kappa \overline{\sigma}_{\bar{x}}. \tag{50}$$

Using (50) and (39) in (46) we have

$$f \hat{u} \approx -\overline{m}_y + \overline{\sigma}^{-1} \kappa f \overline{\sigma}_{\bar{x}} - \mu^2 \hat{v}. \tag{51}$$

Reverting to level coordinates, we can rewrite (51) as

$$f \hat{u} \approx -\overline{p}_y - \kappa f (\overline{b}_x / \overline{b}_z)_z - \mu^2 \hat{v}. \tag{52}$$

At the eastern boundary, \hat{u} must vanish, and so does the rhs of (52). From (44), $\mu^2 \hat{v}$ has no vertical average, we thus integrate (52) to obtain a relation equivalent to that of Sumata and Kubokawa (2001), that is,

$$\int_{-h}^0 \overline{p}_y dz = \kappa f (\overline{b}_x / \overline{b}_z)|_{z=-h} \quad \text{at } x = x_e, \tag{53}$$

where we have used the boundary condition $\overline{b} = \overline{b}_s(y)$ at $z = 0$. In the limit $\kappa \rightarrow 0$, the relation found by Sumata and Kubokawa (2001) is recovered, which gives either $\overline{p}_y = 0$ at $x = x_e$ or a scaleless relation equivalent to (4). However, with eddies, (53) in combination with (49) provides an explicit scale for h . The relation (53) also shows that, insofar as the across-shore eddy transport of buoyancy can be parameterized as a downgradient flux, there is indeed a connection between the alongshore pressure gradient and the across-shore buoyancy gradient, which, in turn, is in thermal wind balance with the alongshore velocity. Therefore, at least in the context of the parameterization (50), the eddy transport of buoyancy necessary to keep the flow adiabatic generates a baroclinic alongshore current, and this gradient also maintains an alongshore pressure gradient.

To derive the scaling for h , we assume an idealized profile of b , which contains the observed features, that is, it satisfies the conditions $\overline{b} = \overline{b}_s$ at the surface, it is stratified with a density jump at $z = -h$, and has a boundary layer modulation on the horizontal scale ℓ . Thus, we make the ansatz

$$\begin{aligned} \overline{b} &= \overline{b}_s(y) + N^2(x, y) z \quad \text{and} \\ N^2(x) &= \alpha \frac{[\overline{b}_s(y) - b_A]}{h} (1 + \gamma e^{x/\ell}), \quad \text{if } -h < z < 0, \end{aligned} \tag{54}$$

where α and γ are nondimensional constants of order unity, and ℓ is given by (49). In particular, $0 < \alpha < 1$ is a nondimensional constant measuring the density jump at $z = -h$ in the interior.

With the ansatz (54), it is possible to calculate h , and compare it with the laminar prediction. The mean pressure at the eastern boundary \overline{p}_e is given by

$$\overline{p}_e = \overline{b}_s(z + h) + \alpha(1 + \gamma)(\overline{b}_s - b_A) \left(\frac{z^2}{2h} - \frac{h}{2} \right) - b_A h. \tag{55}$$

Taking the buoyancy below the thermocline b_A to be constant, substituting (54) and (55) into (53), and evaluating at the eastern boundary, we find

⁶ To obtain (47) we assume $(\overline{\sigma' m'_y})_{\bar{x}} \sim \sigma'_x m'_y$. If the eddies are geostrophic and hydrostatic eddies, then $m'_y \sim f u'$ and $\sigma'_x \sim f v'_{bb}$.

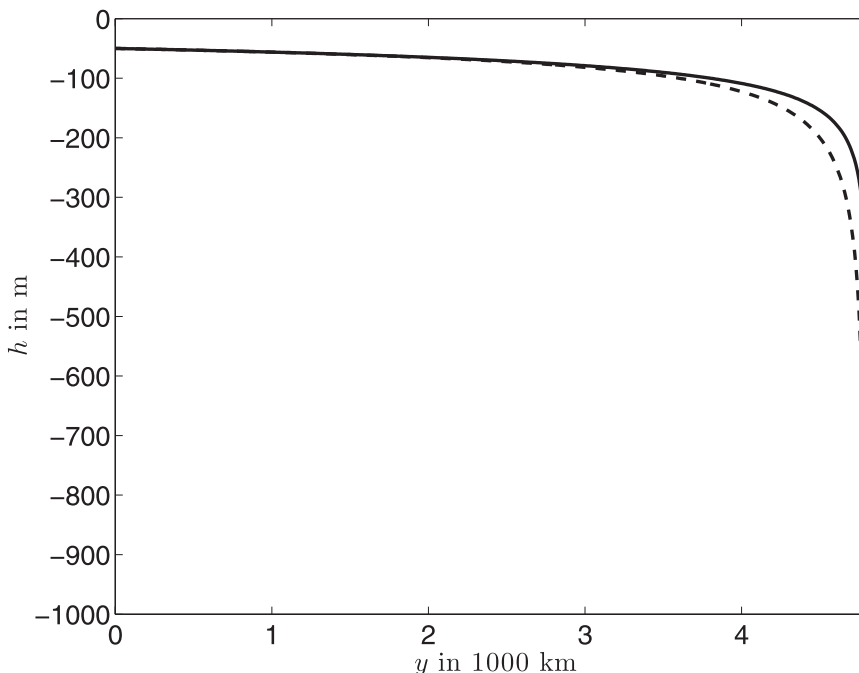


FIG. 15. The expression for h given in (58) is plotted as a function of y in the two limits, $h_o = 0$ (solid) and $\kappa = 0$ (dashed) for the parameter values given in (60).

$$[(\bar{b}_s - b_A)h^2]_y = -c\kappa f^2 [(\bar{b}_s - b_A)h^2]^{1/4} (\bar{b}_s - b_A)^{-3/4}, \tag{56}$$

where c is a nondimensional positive constant with an uninteresting combination of α and γ . Taking

$$\bar{b}_s - b_A = B_o(1 - y/L), \tag{57}$$

where L is the northern limit of the domain, we can integrate (56) to find

$$h = \left[\frac{h_o^{3/2}}{(1 - y/L)^{3/4}} + C \frac{\kappa\beta^2 L^3}{B_o^{3/2}} \frac{q(y/L)}{(1 - y/L)^{1/2}} \right]^{2/3}, \tag{58}$$

where C is another nondimensional constant that depends on α and γ , h_o is the scale that needs to be specified in the framework of Sumata and Kubokawa (2001) and $q = 32 + 8y/L + 5(y/L)^2$ is a weakly varying function of latitude. We are now in a position to contrast the two limits $\kappa = 0$ (Sumata and Kubokawa 2001) and $h_o = 0$. The first limit recovers (4), where the scale of h needs to be specified at some latitude (here, $y = 0$), and there is no dependence given in terms of the external parameters. The second limit gives

$$h \sim \frac{(\kappa\beta^2)^{2/3} L^2}{B_o} (1 - y/L)^{-1/3}. \tag{59}$$

The two predictions, one for $h_o = 0$ and one for $\kappa = 0$, are shown in Fig. 15, for the following set of parameters:

$$\begin{aligned} \beta &= 2 \times 10^{-11} \text{ m}^{-1} \text{ s}^{-1}, & L &= 4.8 \times 10^6 \text{ m}, \\ B_o &= 0.03 \text{ m s}^{-2}, & \kappa &= 1000 \text{ m}^2 \text{ s}^{-1}, & \text{and} \\ h_o &= 50 \text{ m}. \end{aligned} \tag{60}$$

To construct Fig. 15, the constant C has been chosen to match the values of h at $y = 0$. The point is that there are only small differences between the two predictions (and neither does a very good job of approximating the location of the stratification maximum shown in Fig. 4), but there is a fundamental difference in the dependence on parameters. Because (59) depends on the poorly constrained value of the eddy diffusivity, it is not an entirely satisfactory scaling. Nevertheless, it makes explicitly the point that the width and depth of the EBC rely on eddy processes.

The wind stress does not appear explicitly in the scaling for h , but it does so implicitly because the time-averaged surface buoyancy \bar{b}_s depends on the surface velocity, which depends on the wind stress (and its curl). As noted earlier, \bar{b}_s reflects a distortion of the imposed surface buoyancy by the wind-driven gyres, leading, inter alia, to a reduced, and even reversed, meridional temperature gradient in the tropical region (cf. Fig. 2).

8. Conclusions

We have demonstrated that eastern boundary currents are part of the general oceanic circulation and not necessarily locally driven by alongshore winds or buoyancy gradients or steered by local shelf topography. The EBCs occur as a result of the eddy fluxes of buoyancy and momentum associated with the baroclinic instability that develops in response to the singularity at the eastern boundary predicted by adiabatic, laminar thermocline theories (Luyten et al. 1983; Pedlosky and Young 1983; Gill 1985). This singularity is the result of the opposing needs to have meridional gradients of buoyancy at the surface, but no flow normal to the boundary. The constraint that the flow remains geostrophic all the way to the wall implies that all the buoyancy surfaces outcrop on the eastern boundary. This configuration creates a “shadow zone” with a large supply of available potential energy, which is released by time-dependent mesoscale eddies. Eddy fluxes of buoyancy slump the buoyancy surfaces on the eastern wall, creating a finite-depth region of meridional pressure gradients. Time-dependence and the associated eddy fluxes of thickness and momentum break the geostrophic balance, allowing the no normal flow condition to be satisfied. It is not necessary to invoke diabatic and viscous processes to maintain a region of gradients and the associated meridional baroclinic boundary current.

Except in the tropics, EBCs are not associated with a net vertical transport of buoyancy—the mean downwelling near the eastern boundary is balanced by an equal and opposite eddy flux of buoyancy, so as to maintain an adiabatic buoyancy balance. Eddy thickness fluxes also alter the mean zonal transport on buoyancy surfaces, so that the zonal flow does not reverse with depth (cf. the top row, rhs in Fig. 8). In the absence of diapycnal exchange this net zonal flow impinging into the coast can only be accommodated by a meridional current, and this creates the EBC.

In addition to eddy fluxes of buoyancy, eddy fluxes of meridional momentum are also created, and these two quantities largely balance each other, so as to produce a small divergence of across-shore PV flux. This balance can be seen by analyzing the PV dynamics or, equivalently, the thickness-weighted averaged alongshore momentum balance (Young 2012). The net result is a confined, baroclinic meridional current whose width is the Rossby deformation radius. The eddy fluxes of buoyancy and momentum, the meridional current, and the meridional pressure gradient on the eastern boundary extend downward to a depth that depends on the eddy buoyancy flux, and inversely with the stratification. These two scales are qualitatively different from those proposed

by Cessi and Wolfe (2009b) and Cessi et al. (2010), l and h_{CWL} , defined as

$$l \equiv \left(\frac{\beta L^2 \kappa}{N^2 \kappa_v} \right)^{1/3} \quad \text{and} \quad h_{\text{CWL}} \equiv \left(\frac{\beta L^2 \sqrt{\kappa \kappa_v}}{N^2} \right)^{1/3}, \quad (61)$$

where κ_v is the diapycnal diffusivity, a quantity that does not enter the scaling proposed here. The scales in Cessi and Wolfe (2009b) and Cessi et al. (2010) are realized in models that parameterize eddies as isopycnal diffusion and do not permit the development of eddies and the associated momentum flux. For standard values of the parameters, l is on the order of 100 km, much larger than the width of the eastern boundary current found here. Given our result that the EBC has a width of the same order of the eddy's scale, the appropriateness of flux-gradient relations relying on scale separation is unclear.

The adiabatic cancellation between mean and eddy buoyancy fluxes is not complete; there are weak diabatic effects in the swash (our model does not have an explicit mixed layer) that lead to heat flux out of (into) the ocean poleward (equatorward) of the interface between the subtropical and tropical gyre, located at approximately $y = 1200$ km (cf. the change in sign of the vertical velocity shown in Fig. 3b). These surface heat fluxes are caused by the heat transport by the surface expression of the EBC that carries warm (cold) water poleward (equatorward) north (south) of said interface. This is the opposite of what it is found in the surface expression of some EBC systems, such as the California Current, where the meridional component of the wind stress near the coast is large enough to overcome the surface poleward EBC.

In the region of the cyclonic tropical gyre, the Ekman suction confines the interior circulation and the EBC to the surface, and diabatic effects are important throughout the depth of the EBC. This results in an eastern boundary-enhanced positive heat flux into the ocean (a cooling of the atmosphere), which is on the same order of the heat loss in the western boundary current (cf. Fig. 16). Clearly, the adiabatic dynamics found in the subtropical and subpolar regions do not apply in the region of tropical upwelling.

The adiabatic, eddy-mediated dynamics found in our simple model should also operate in more realistic domain geometry and forcing. Indeed, Colas et al. (2013) find a similar cancellation between mean and eddy transport of buoyancy in a realistic regional model of EBCs off of California, Peru, and Chile. Colas et al. (2013) report a more substantial breakdown in adiabaticity in the near-surface layer than ours; this could be because of their more explicit mixed layer model, or the

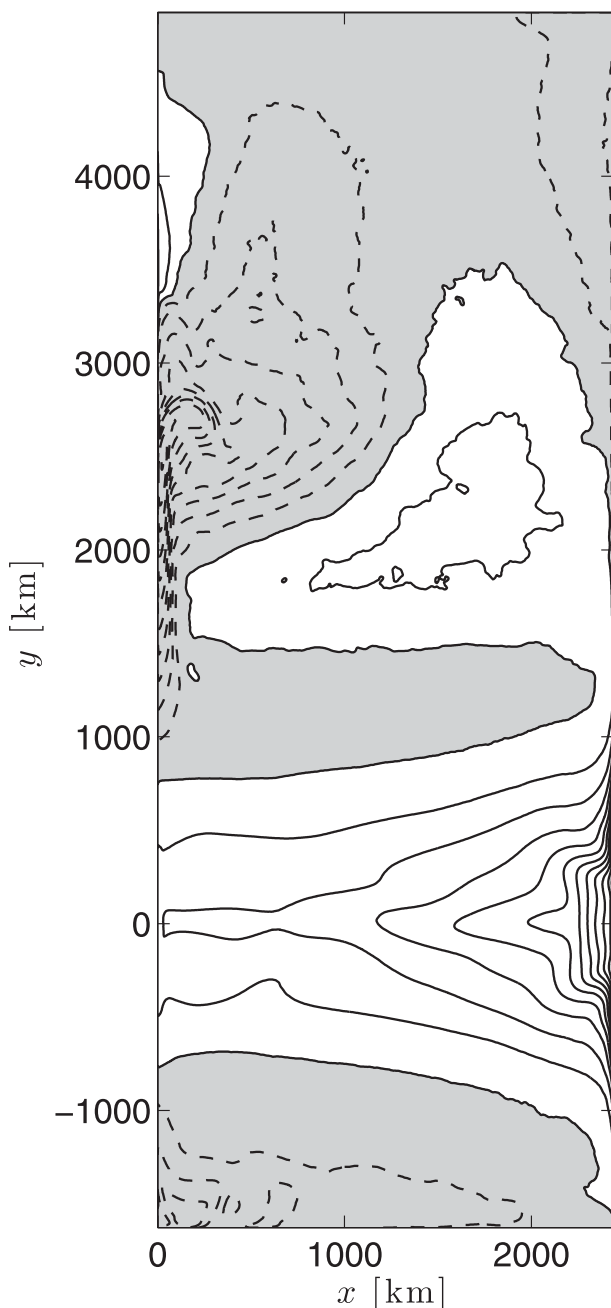


FIG. 16. The air-sea heat flux (W m^{-2}) as a function of x and y . The sign convention is that positive indicates a heating into the ocean.

locally wind-forced upwelling which promotes air-sea heat fluxes, or to the difference in diagnostics, in particular the already noted difference between \hat{w} and $w^\#$ (cf. the bottom rows of Figs. 6 and 8).

We conjecture that if we added a near-coast southward component of the wind stress, a shallow equatorward current would be superposed on top of the EBC described so far, but the dynamics of the subsurface

equatorward current would still be inviscid and adiabatic.

Acknowledgments. Our research is supported by the Office of Science Biological and Environmental Research, U.S. Department of Energy, Grants DE-SC0001962 and DE-SC0005100. Computational resources were provided by the National Energy Research Scientific Computing Center. We are very grateful to the anonymous referees for their constructive reviews.

REFERENCES

- Barton, E. D., 1998: Eastern boundary of the North Atlantic: Northwest Africa and Iberia. *The Sea—Ideas and Observations on Progress in the Study of the Seas*, A. R. Robinson and K. H. Brink, Eds., *The Composition of Sea-Water and Comparative and Descriptive Oceanography*, Vol. 2, Wiley and Sons, 633–657.
- Cessi, P., and C. L. Wolfe, 2009a: Eddy-driven buoyancy gradients on eastern boundaries and their role in the thermocline. *J. Phys. Oceanogr.*, **39**, 1595–1614.
- , and —, 2009b: Eddy-driven buoyancy gradients on eastern boundaries and their role in the thermocline. *J. Phys. Oceanogr.*, **39**, 1595–1614.
- , —, and B. Ludka, 2010: Eastern-boundary contribution to the residual and meridional overturning circulations. *J. Phys. Oceanogr.*, **40**, 2075–2090.
- Chapman, D. C., and S. J. Lentz, 2005: Acceleration of a stratified current over a sloping bottom, driven by an alongshelf pressure gradient. *J. Phys. Oceanogr.*, **25**, 1305–1317.
- Chelton, D., R. DeSzoeke, M. Schlax, K. El Naggar, and N. Siwertz, 1998: Geographical variability of the first baroclinic Rossby radius of deformation. *J. Phys. Oceanogr.*, **28**, 433–460.
- Colas, F., X. Capet, J. C. McWilliams, and Z. Li, 2013: Mesoscale eddy buoyancy flux and eddy-induced circulation in Eastern Boundary Currents. *J. Phys. Oceanogr.*, in press.
- Colin de Verdière, A., 1989: On the interaction of wind and buoyancy driven gyres. *J. Mar. Res.*, **47**, 595–633.
- Daru, V., and C. Tenaud, 2003: High order one-step monotonicity-preserving schemes for unsteady compressible flow calculations. *J. Comput. Phys.*, **193**, 563–594.
- De Szoeke, R., and A. Bennett, 1993: Microstructure fluxes across density surfaces. *J. Phys. Oceanogr.*, **23**, 2254–2264.
- Feng, M., S. Wijffels, S. Godfrey, and G. Meyers, 2005: Do eddies play a role in the momentum balance of the Leeuwin Current? *J. Phys. Oceanogr.*, **25**, 964–975.
- Gill, A. E., 1985: An explicit solution of the linear thermocline equations. *Tellus*, **37A**, 276–285.
- Godfrey, J. S., and K. Ridgway, 1985: The large-scale environment of the poleward-flowing Leeuwin Current, western Australia: Alongshore steric height gradients, wind stresses, and geostrophic flow. *J. Phys. Oceanogr.*, **15**, 481–495.
- , and A. Weaver, 1991: Buoyancy driven planetary flows. *Prog. Oceanogr.*, **27**, 225–272.
- Luyten, J., J. Pedlosky, and H. Stommel, 1983: The ventilated thermocline. *J. Phys. Oceanogr.*, **13**, 292–309.
- Marchesiello, P., J. McWilliams, and A. Skhepetkin, 2003: Equilibrium structure and dynamics of the California Current system. *J. Phys. Oceanogr.*, **33**, 753–783.

- Marotzke, J., 1997: Boundary mixing and the dynamics of three-dimensional thermohaline circulations. *J. Phys. Oceanogr.*, **27**, 1713–1728.
- McCreary, J. P., 1981: A linear stratified ocean model of the coastal undercurrent. *Philos. Trans. Roy. Soc. London*, **A302**, 385–413.
- McDougall, T., and P. McIntosh, 1996: The temporal-residual-mean velocity. Part I: Derivation and the scalar conservation equations. *J. Phys. Oceanogr.*, **26**, 2653–2665.
- , and —, 2001: The temporal-residual-mean velocity. Part II: Isopycnal interpretation and the tracer and momentum equations. *J. Phys. Oceanogr.*, **31**, 1222–1246.
- Pedlosky, J., and W. R. Young, 1983: Ventilation, potential vorticity homogenization and the structure of the ocean circulation. *J. Phys. Oceanogr.*, **13**, 2020–2037.
- , and M. A. Spall, 2005: Boundary intensification of vertical velocity in a β -plane basin. *J. Phys. Oceanogr.*, **35**, 2487–2500.
- Penven, P., V. Echevin, J. Pasapera, F. Colas, and J. Tam, 2005: Average circulation, seasonal cycle, and mesoscale dynamics of the Peru Current System: A modeling approach. *J. Geophys. Res.*, **110**, C10021, doi:10.1029/2005JC002945.
- Pierce, S. D., R. L. Smith, P. M. Kosro, and J. A. B. C. D. Wilson, 2000: Continuity of the poleward undercurrent along the eastern boundary of the mid-latitude North Pacific. *Deep-Sea Res. II*, **47**, 811–829.
- Rhines, P. B., and W. R. Young, 1982: A theory of the wind-driven circulation. I: Mid-ocean gyres. *J. Mar. Res.*, **40** (Suppl.), 559–596.
- Rienecker, M. M., and L. L. Ehret, 1988: Wind stress curl variability over the North Pacific from the Comprehensive Ocean–Atmosphere Data Set. *J. Geophys. Res.*, **93** (C5), 5069–5077.
- Schloesser, F., R. Furue, J. McCreary, and A. Timmermann, 2012: Dynamics of the Atlantic meridional overturning circulation. Part 1: Buoyancy-forced response. *Prog. Oceanogr.*, **101**, 33–62.
- Smith, R. L., A. Huyer, J. S. Godfrey, and J. A. Church, 1991: The Leeuwin Current off Western Australia, 1986/87. *J. Phys. Oceanogr.*, **21**, 323–345.
- Spall, M., 2010: Dynamics of downwelling in an eddy-resolving convective basin. *J. Phys. Oceanogr.*, **40**, 2341–2347.
- , and R. Pickart, 2001: Where does dense water sink? A sub-polar gyre example. *J. Phys. Oceanogr.*, **31**, 810–826.
- Sumata, H., and A. Kubokawa, 2001: Numerical study of eastern boundary ventilation and its effects on the thermocline structure. *J. Phys. Oceanogr.*, **31**, 3002–3019.
- Todd, R., D. Rudnick, M. Mazloff, R. Davis, and B. Cornuelle, 2011: Poleward flows in the southern California current system: Glider observations and numerical simulation. *J. Geophys. Res.*, **116**, C02026, doi:10.1029/2010JC006536.
- , —, —, B. Cornuelle, and R. Davis, 2012: Thermohaline structure in the California Current System: Observations and modeling of spice variance. *J. Geophys. Res.*, **117**, C02008, doi:10.1029/2011JC007589.
- Young, W. R., 2012: An exact thickness-weighted average formulation of the Boussinesq equations. *J. Phys. Oceanogr.*, **42**, 692–707.